Applied Mathematical Modelling 96 (2021) 152–176

Contents lists available at ScienceDirect

Applied Mathematical Modelling

journal homepage: www.elsevier.com/locate/apm

Heart rhythm analysis using a nonlinear dynamics perspective

Augusto Cheffer[a], Marcelo A. Savi[a,*], Tiago Leite Pereira[b], Aline Souza de Paula[b]

[a] COPPE – Department of Mechanical Engineering, Center for Nonlinear Mechanics, Universidade Federal do Rio de Janeiro, P.O. Box 68.503, 21.941.972, Rio de Janeiro, RJ, Brazil
[b] Department of Mechanical Engineering, Universidade de Brasília, 70.910.900, Rio de Janeiro, RJ, Brazil

ARTICLE INFO

Article history:
Received 17 September 2020
Revised 26 February 2021
Accepted 2 March 2021
Available online 11 March 2021

Keywords:
Nonlinear dynamics
Chaos
Cardiac rhythms
Poincaré maps
Bifurcations
Biomechanics

ABSTRACT

Biological rhythms are fundamental for the understanding of the physiological functioning of organisms, being useful in disease prevention and treatments. This work deals with the analysis of cardiac rhythms evaluating the electrical activity of the heart based on ECG observations. A mathematical model composed by three nonlinear oscillators coupled by time-delayed connections is employed for heartbeat description. Numerical simulations reproduce synthetic ECGs with a broad variety of responses, including normal and pathological rhythms. Atrial flutter, atrial fibrillation, ventricular flutter and two different kinds of ventricular fibrillation are investigated showing the model capability to capture the general functioning of the heart dynamics. Nonlinear tools are employed in order to help the physiology understanding, being potential interesting to help the characterization of the different behaviors. In this regard, Poincaré maps and bifurcation analysis are of concern. Poincaré maps can highlight dynamical characteristics of each rhythm while bifurcation analysis can be useful to investigate the routes from normal functioning to pathologies, which can be useful to establish an early identification of critical situations. In general, results show that dynamical perspective can be useful for physiology comprehension that can also help to pathology characterization.

1. Introduction

Natural phenomena have essential nonlinear characteristics responsible for the variety and richness of behaviors. Rhythms constitute one of the most relevant manifestations of natural systems being possible to be regular or irregular in time and space. In this regard, periodic and non-periodic dynamics can be related to either normal or pathological physiological functioning. This idea motivates the natural system analysis through a dynamical perspective that usually can be performed based on either mathematical models or time series analysis [1].

The cardiac system is one of the possibilities where dynamical perspective has showing to be useful, being applicable either for clinical or chaos control purposes. In brief, heart is a muscular organ activated by electrical stimuli with the function of pumping blood through all the organs and tissues of the body. In mammals, the heart is divided into 4 cavities: 2 atria and 2 ventricles. The conduction of the electrical impulse in the cardiac system can be understood as a complex network of self-excitatory elements. A reduced-order description can be imagined by considering a network formed by sinoatrial node (SA), atrioventricular node (AV) and His-Purkinje complex (HP) [2,3]. The initial excitation occurs in the

* Corresponding author.
E-mail addresses: augusto.cheffer@poli.ufrj.br (A. Cheffer), savi@mecanica.ufrj.br (M.A. Savi), alinedepaula@unb.br (A.S. de Paula).

https://doi.org/10.1016/j.apm.2021.03.014
0307-904X/

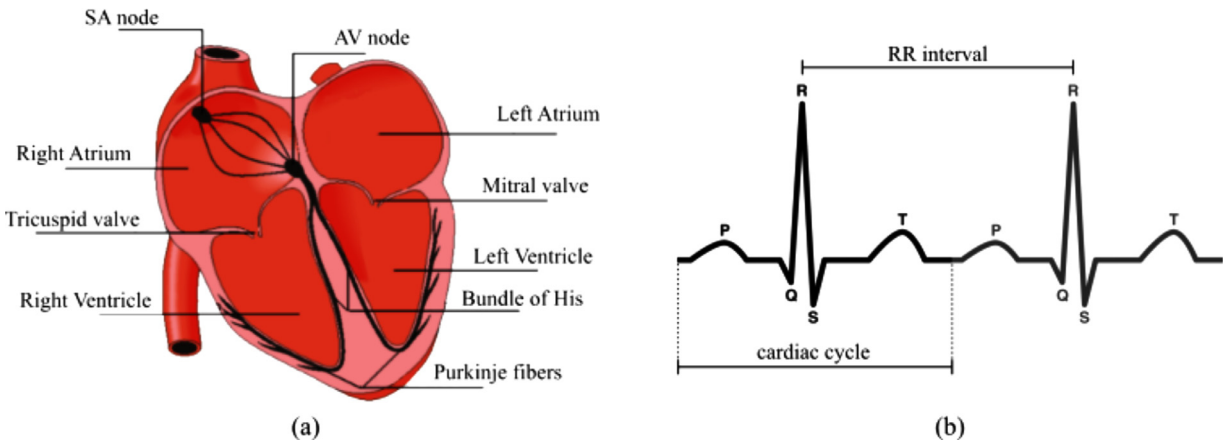

Fig. 1. Heart and typical response. (a) Heart anatomy; (b) ECG response representing a normal cardiac cycle characterized by three important components: P wave, QRS complex and T wave. P wave represents the impulse generated by the SA node. The QRS complex is formed by ventricular contraction. T wave reflects ventricular repolarization. Heart rate variability illustrated by RR interval is also represented.

SA node, natural pacemaker, and propagates as a wave, stimulating atria. Upon reaching the AV node, it initiates a pulse that excites the bundle of His and, afterward, the Purkinje fibers. The fibers distribute the stimulus to the myocardial cells, causing the ventricles contraction [4].

The electrocardiogram (ECG) records the electrical activity of the heart being useful to analyze its behavior, inferring heartbeat rate and regularity. ECG has a widespread use due to its non-invasive characteristics. Basically, the electrical impulses generated during cardiac functioning are recorded in the form of waves, which characterize the electrical current in different areas of the heart. Fig. 1 shows a schematic picture of a heart and an ECG normal cardiac cycle. Three important components should be pointed out: P wave, QRS complex and T wave. P wave represents the impulse generated by the SA node. The QRS complex is formed by ventricular contraction. T wave reflects ventricular repolarization when cardiac cells return to state in which they are ready to react to another stimulus. Although normal ECG is apparently periodic, it is usual to present heart rate variability (HRV) that can be measured from R-R intervals [5].

The analysis of the cardiac dynamics from mathematical models can be performed by different ways. Moe et al. [6] proposed a model that represents the atrial tissue behavior under fibrillation based on a finite number of hexagonal elements with five different states of excitability. Krinsky [7] presented a mathematical study indicating the causes of arrhythmias by considering five main aspects: re-entry; vulnerability; mechanisms for initiation, development and termination of fibrillation; 'critical mass' of fibrillation; and modes of action of antiarrhythmic drugs.

Fenton and Karma [8] presented an ionic model with three membrane currents that represents the restitution properties and spiral wave behaviors of cardiac action potential (AP). A semi-implicit algorithm is employed for the solution of 1D-domain equations with rotational anisotropy. Jalife et al. [9] presented a unified hypothesis that sustained atrial fibrillation (AF) depends on the uninterrupted periodic activity of discrete reentrant sites. Fenton et al. [10] developed a simplified ionic model of the cardiac AP that approximates a wide variety of experimental data based on the mesoscopic characteristics of the cardiac tissue, allowing the explanation of several mechanisms of spiral wave breakup that can occur in the cardiac tissue. McSharry et al. [11] presented a model based on a set of three ordinary differential equations to generate synthetic ECG signals. It also considered the respiratory sinus arrhythmia (RSA) where the frequency is calculated from a power spectrum with two Gaussian distributions. Mitchell and Schaeffer [12] introduced a model for ventricular cardiac membrane dynamics consisting of two temporal functions, representing the membrane potential and current gating variable, both employing a first order ordinary differential equation. Nash and Panfilov [13] presented an excitable tissue model capable of conducting nonlinear excitation waves, using a constitutive model of the deformed tissue. This model is able to reproduce reentry mechanisms that occur in arrhythmias such as flutter and fibrillation.

Reduced-order models are interesting to analyze some aspects of heart dynamics, being the objective of several researches since the pioneer work of Van der Pol & Van der Mark [14] that established an analogy between heartbeats and electronic circuits represented by nonlinear oscillators. Grudzinski and Zebrowski [15] proposed alterations on the original Van der Pol (VdP) oscillator in order to present a more suitable description of the natural pacemaker. Dos Santos et al. [16] modeled cardiac dynamics considering two asymmetrically coupled modified VdP oscillators, representing the behavior of the two cardiac pacemakers, SA and AV nodules. Gois and Savi [2] proposed a three-coupled oscillator model in order to represent ECG signals. Besides, SA and AV nodules, His-Purkinje complex (HP) is also considered on system modeling. Each oscillator is based on the model due to [15] and the system has bidirectional and asymmetric time-delayed couplings to represent the time spent on impulse transmissions. Cheffer and Savi [17] improved the three-coupled oscillator model due to [2] model incorporating nondeterministic aspects by considering random connections among oscillators. The main idea is to show that nonlinearities and randomness define together the great variety of possibilities in the heart dynamical system.

Ryzhii and Ryzhii [18,19] presented a model that considers heart pacemakers as a network of strongly asymmetric VdP oscillators connected with unidirectional time delay couplings. Cardiac muscle depolarization and repolarization waves are modeled using separate FitzHugh-Nagumo (FHN) type equations. Motivated by the improvement of the description of the branch block and based on FHN equations, Cardarilli et al. [20] proposed a model with four modified VdP oscillators representing the groups: SA and AV nodes, Right and Left bundle branches. Son et al. [21] presented a stochastic cardiovascular-pump model to describe effects of left ventricular assisted devices on heart hemodynamics.

Sato et al. [22] modeled the cardiac action potential including cooperative gating of L-type $Ca_V1.2$ channels (LTCC) and added the complexity of this gating phenomenon to the existing models. In addition, the effects of cooperative gating on alternans were included obtaining results in agreement with experimental data [23]. This work concluded that the model can reproduce experimental data by considering the effects of changes in the strength of cooperative gating of LTCCs on L-type Ca2+ currents. Quiroz-Juarez et al. [24] treated a three nonlinear oscillator system that simulate the main cardiac pacemakers. The model is derived from a discretized reaction-diffusion system, being able to describe ECGs of healthy and pathological responses. Pathmanathan et al. [25] proposed a cardiac action potential model considering six currents, seven variables and 36 parameters. They also prescribed input variability for all parameters. Besides that, uncertainty quantification and sensitivity analysis are performed for a range of model-derived quantities with physiological relevance and discussed quantitative and qualitative strategies to analyze different behaviors that occur under parameter uncertainty, including model failure.

The analysis of the cardiac system dynamics can be alternatively performed by time series analysis. The idea is to build a model from time series, usually ECGs. The unavoidable noise contamination demands reliable signal processing techniques [26]. Some of these procedures include detection of R-peaks [27,28] and calculation of heart rate variability and breathing [5,29].

Some studies treat aspects of ventricular fibrillation (VF) by different approaches including frequency analysis of canine ECGs [30], computerized mapping techniques of physiological mechanisms [31] and spatial organization quantification techniques in ECGs of pigs [32]. Jalife [33] provided a historical review and highlights of the literature of mechanisms of initiation and support of ventricular fibrillation. Beyond that, supported by experimental data, the authors discussed the hypothesis that ventricular fibrillation in physiologically normal heart is not a pure random response. Nannes et al. [34] observed the presence of critical slowing down (CSD) in patients with ventricular fibrillation showing that critical slowing down is a buildup autocorrelation from ECGs that can be employed as a warning indicator for critical transitions. Skanes et al. [35] identified the presence of spatial and temporal periodicity during atrial fibrillation observing ECG recordings and spectral analysis of sheep hearts.

The influence of external factors on the HRV, as breathing and physical effort, is the subject of several studies. Krstacic et al. [36] highlighted clinical significance of ECG changes in short time series of patients with coronary heart disease during exercise. Ernst & Bar-Joseph [37] developed a software for the analysis of short time series, called short time series expression miner (STEM). Tobón et al. [38] proposed a new method to HRV analysis for highly noised ECG signals, called modulation domain HRV. This method is based on a spectro-temporal ECG representation, separating cardiac components from artifacts. Shiraishi et al. [39] developed a HVR analysis that provides a real time visualization of power spectra during physical exercises. Experimental data were measured from a group composed of healthy individuals and people with history of heart attack. Wang et al. [40] investigated differences between normal sinus rhythm and congestive heart failure by applying three approaches: time-domain, frequency-domain and non-linear indexes. Hu et al. [41] developed a method based on seven time-scales to identify normal sinus rhythm and congestive heart failure using HRV measures of Physio Bank data. Ueno et al. [42] employed Malthusian parameter and recurrence plots in order to investigate correlations between numerical results of the model due to [2] and experimental data (PhysioBank). Costa and Goldberger [43] explored the use of a set of dynamical biomarkers associated with the influence of biological aging over cardiac dynamics.

The use of neural networks is another tool associated with relevant contributions. Deng et al. [44] proposed a dynamical ECG recognition framework for human identification and cardiovascular diseases classification via a dynamical neural learning mechanism. Silvestri et al. [45] applied neural networks to obtain parameters that satisfy desired ECG signal features employing the model due to [18]. This procedure allows to build synthetic ECGs without a deep knowledge of the mathematical model. Khan et al. [46] studied the conditionality of a VdP model by applying artificial neural networks. The procedure consists by a combination of a global search technique, the Harris Hawks optimizer and a local search technique, the interior point algorithm.

An important and relevant discussion about heart dynamics is related to its deterministic and random aspects. Kaplan and Cohen [47] analyzed canine ECGs with fibrillation and verified that these responses are similar to random signals. Nevertheless, a deterministic dynamical system can generate similar random-looking, nonchaotic behavior. Yates and Benton [48] pointed the main challenges about the deterministic and statistical analysis of the human cardiac data treatment. Christini et al. [49] employed an autoregressive model based on power spectra on experimental and synthetic heart rhythm time series. Monte Carlo simulations are employed where autoregressive model parameters are subjected to Gaussian distributions. Bozoki [50] developed a data acquisition method for fetal heart rate suitable either to power spectral analysis (statistical) or chaos theory (deterministic). Kantz and Schreiber [51] presented a comparison between deterministic chaos and random noise for cardiac rhythm analysis. Based on the model due to [11], Evaristo et al. [52] calculated the RSA frequency by using an autoregressive process, using Poincaré maps to compare results with experimental data and numerical simulations.

Several papers investigated external factors and couplings evaluating their influence on HRV. Glass [3] highlighted stochastic stimulus influence, respiratory influence and multiple feedback circuits. Zhang et al. [53] showed that the stochastic release of the acetylcholine regulator in the vicinity of the SA node leads to a chaotic rhythm using a theoretical modulation model of normal sinus rhythm. Wessel et al. [54] employed regression methods to investigate coupling between respiratory and heartbeat rates and concluded that the HRV is directly caused by fluctuations on respiratory rate. Buchner et al. [55] investigated the bidirectional coupling between respiration and cardiac rates using stochastic methods.

Johnstone et al. [56] discussed uncertainty quantification and its application to the analysis of ECG models. They also provided an overview of the currents that can cause HRV, based on probability distributions across data of canine APs. Aronis et al. [57] concluded that heart rhythm does not consist of a rescaled linear stochastic process or a fractional noise based on symbolic analysis in atrial fibrillation surrogate data. Jawarneh and Staffeldt [58] developed a study of bifurcations on a modified VdP oscillator applying Conley index methods.

The control of cardiac rhythms has been exploited by considering different approaches. Garfinkel et al. [59,60] presented the first experiment of chaos control on biomechanical systems, applying OGY method [61] on rabbit cardiac muscle. Ferreira et al. [62] employed time-delayed feedback control for natural pacemaker using a model proposed by [15]. Afterward, Ferreira et al. [63] employed the same technique for ECG signals built with a three-coupled oscillators [2]. Results showed stabilization of unstable periodic orbits embedded on chaotic attractors, avoiding critical situations. Lounis et al. [64] applied high-order control method due to Quiroz-Juarez et al. [65] model considering the stabilization of a desired unstable periodic orbit (UPO). Khan and Nigar [66] proposed an active control technique based on Lyapunov stability theory, considering the combination of projective synchronization in fractional-order chaotic system with disturbance and uncertainty.

This paper deals with the analysis of the heart physiology, through its electrical activity, using a nonlinear dynamics perspective. Mathematical description considers a reduced-order model proposed to represent the cardiac functioning in order to generate synthetic ECG signals. The model is based on the one proposed by Gois & Savi [2], being altered to consider different coupling terms. Essentially, the model has three-coupled nonlinear oscillators with delayed connection. It is represented by delayed differential equations being able to capture the main aspects of the ECGs representing normal and pathological rhythms. The new model increases the capability to describe pathological behaviors and allows quantitative comparisons between experimental and numerical data. Besides the proposition of the new model, the main contribution of this paper is the use of nonlinear tools as potential candidates to aid the rhythm identification that, ultimately, can be useful for diagnosis purposes. Poincaré map is used in order to highlight the pathological characteristics. Different procedures are employed to build Poincaré maps. Afterward, a bifurcation analysis is conducted, establishing different conditions of the routes from normal to pathological behaviors. Since pathological behaviors can be understood as dynamical diseases, the effect of parameter variations is of special interesting, which justify the bifurcation analysis. Results show that Poincaré maps and bifurcation diagrams are interesting potential candidates to help heart dynamical analysis.

After this introduction, the paper is organized as follows. Pacemaker and cardiac system mathematical models are presented. Numerical simulations are presented showing some heart behaviors and highlighting physiological aspects and their effects on ECG. Two procedures to build Poincaré map are presented and applied. Bifurcation analysis is investigated considering different routes to pathological behaviors. Finally, conclusions are discussed.

2. Mathematical modeling

The mathematical modeling of the natural pacemaker is the starting point for cardiac modeling. Van der Pol oscillator is often used in the modeling of cardiac functions because its dynamic response presents typical characteristics of biological systems such as: limit cycle, synchronization and chaos [2,15]. Besides that, Van der Pol equation has oscillation amplitude that does not depend of the oscillation rate. The model proposed by [15] is a modification of the original Van der Pol oscillator replacing the restitution force by a cubic function being expressed as follows:

$$\ddot{x} + \alpha\dot{x}(x-\nu_1)(x-\nu_2) + \frac{x(x+d)(x+e)}{d\ e} = F(t) \tag{1}$$

where α defines the pulse shape, characterizing the time when the heart receives the stimulus; ν_1 and ν_2 determine the signal amplitude, and to preserve the self-excitatory nature, $\nu_1\nu_2 < 0$; and $F(t)$ is an external stimulus.

The stability analysis of equilibrium points through the eigenvalues of the Jacobian matrix shows that the system exhibits 3 equilibrium points $(x, \dot{x}) : (0, 0), (-d, 0)$ and $(-e, 0)$, being respectively characterized by center, saddle and stable node [15].

Heart physiology modeling, essentially represented by ECG, can be made by considering reduced-order models from the coupling of three nonlinear oscillators with asymmetrical and bidirectional connections as proposed by [2]. Fig. 2 shows the conceptual model of this approach where it is noticeable situations that do not occur in the normal functioning, representing a general condition of the heart dynamics that includes pathological behaviors. In addition, external stimulus is incorporated as a reduced order model for spatiotemporal stimulus. This external stimulus increases the system dimension based on spatiotemporal information. Therefore, central nervous system stimuli are represented by limit cycle behavior while external stimuli are associated with any input different from the normal functioning.

Therefore, the heart physiology can be modeled by three oscillators (SA, AV and HP) that are coupled by time-delayed terms that represent the transmitting time spent among each one of the oscillators. Each oscillator is described by the model

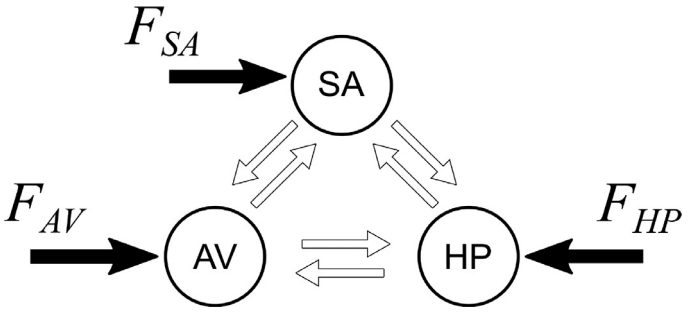

Fig. 2. Conceptual model of the general cardiac functioning represented by sinoatrial node (SA), atrioventricular node (AV) and His-Purkinje complex (HP) with asymmetrical and bidirectional connections. $\boldsymbol{F_{SA}}$,$\boldsymbol{F_{AV}}$ and $\boldsymbol{F_{HP}}$ are external stimuli.

due to [15] and the coupling terms are different from the original model of Gois and Savi [2] by considering independent parameters. This change increases the model capability to describe pathologies being inspired on the observations of some pathological behaviors, notable atrial flutter and fibrillation. Based on that, the synthetic ECG obtained by the model is a result of the behavior of cardiac cells. Therefore, it can be understood as a macroscopic behavior related to the electrical activity of the heart, rather micro or mesoscopic behavior of the heart. Under these assumptions, the system dynamics is governed by the following equations.

$$
\begin{aligned}
\dot{x}_1 &= x_2 \\
\dot{x}_2 &= F_{SA}(t) - \alpha_{SA} x_2 \left(x_1 - \nu_{SA_1}\right)\left(x_1 - \nu_{SA_2}\right) - \frac{x_1(x_1 + d_{SA})(x_1 + e_{SA})}{d_{SA} e_{SA}} \\
&\quad - k_{AV-SA} x_1 + k^{\tau}_{AV-SA} x_3^{\tau_{AV-SA}} - k_{HP-SA} x_1 + k^{\tau}_{HP-SA} x_5^{\tau_{HP-SA}} \\
\dot{x}_3 &= x_4 \\
\dot{x}_4 &= F_{AV}(t) - \alpha_{AV} x_4 \left(x_3 - \nu_{AV_1}\right)\left(x_3 - \nu_{AV_2}\right) - \frac{x_3(x_3 + d_{AV})(x_3 + e_{AV})}{d_{AV} e_{AV}} \\
&\quad - k_{SA-AV} x_3 + k^{\tau}_{SA-AV} x_1^{\tau_{SA-AV}} - k_{HP-AV} x_3 + k^{\tau}_{HP-AV} x_5^{\tau_{HP-AV}} \\
\dot{x}_5 &= x_6 \\
\dot{x}_6 &= F_{HP}(t) - \alpha_{HP} x_6 (x_5 - \nu_{HP_1})(x_5 - \nu_{HP_2}) - \frac{x_5(x_5 + d_{HP})(x_5 + e_{HP})}{d_{HP} e_{HP}} \\
&\quad - k_{SA-HP} x_5 + k^{\tau}_{SA-HP} x_1^{\tau_{SA-HP}} - k_{AV-HP} x_5 + k^{\tau}_{AV-HP} x_3^{\tau_{AV-HP}}
\end{aligned}
\tag{2}
$$

By considering indexes m and n that can represent SA, AV or HP, and $m \neq n$, equation terms are now explained. k_{m-n} and k^{τ}_{m-n} are coupling coefficients between m and n nodes; and $x_i^{\tau_{m-n}} = x_i(t - \tau_{m-n})$ are delayed terms where τ_{m-n} is the time delay. Since the couplings have temporal lags, the system is governed by delayed differential equations (DDEs). Besides, $F_m(t) = \rho_m \sin(\omega_m t)$ is an external excitation that represents spatiotemporal stimulus and therefore, it is considered as a reduced order representation of spatiotemporal aspects. Note that this external stimulus increases the system dimension based on spatiotemporal information.

The electrical activity of the heart, represented by ECG, is formed by the signal of each one of the oscillators, being formed by a linear combination of the state variables given by [2],

$$
X = ECG = X_{SA} + X_{AV} + X_{HP} \tag{3}
$$

where each oscillator is related to the following signals,

$$
\begin{aligned}
X_{SA} &= \frac{\beta_0}{3} + \beta_1 x_1 \\
X_{AV} &= \frac{\beta_0}{3} + \beta_2 x_3 \\
X_{HP} &= \frac{\beta_0}{3} + \beta_3 x_5
\end{aligned}
\tag{4}
$$

where β_0, β_1, β_2 and β_3 are parameters. Therefore,

$$
\dot{X} = \frac{d(ECG)}{dt} = \beta_1 x_2 + \beta_2 x_4 + \beta_3 x_6 \tag{5}
$$

Since governing equations are presented in dimensionless form, it is interesting to define a dimensional time $\bar{t}$ $[s]$: $\bar{t} = \beta_t\ t$, where $[\beta_t] = s$ can be estimated by the ratio between experimental RR interval, RR_{exp}, and numerical RR interval, RR_{num}: $\frac{\text{mean}(RR_{exp})}{\text{mean}(RR_{num})}$.

Table 1
Cardiac system parameters.

	Normal rhythm	Atrial flutter	Atrial fibrillation	Ventricular flutter	Ventricular fibrillation with stimulus	Ventricular fibrillation without stimulus
SA oscillator						
α_{SA}	3	3	3	3	3	3
ν_{SA_1}	1	1.65	1	1	1	1
ν_{SA_2}	− 1.9	− 4.2	− 1.9	− 1.9	− 1.9	−1.9
d_{SA}	1.9	1.9	1.9	1.9	1.9	1.9
e_{SA}	0.55	0.55	0.55	0.55	0.55	0.55
AV oscillator						
α_{AV}	3	7	7	3	3	3
ν_{AV_1}	0.5	0.5	0.5	0.5	0.5	0.5
ν_{AV_2}	− 0.5	− 0.5	− 0.5	− 0.5	− 0.5	− 0.5
d_{AV}	4	4	4	4	4	4
e_{AV}	0.67	0.67	0.67	0.67	0.67	0.67
HP oscillator						
α_{HP}	7	7	7	7	0.5	0.5
ν_{HP_1}	1.65	1.65	1.65	1.65	1.65	1.65
ν_{HP_2}	− 2	− 2	− 2	− 2	− 2	− 2
d_{HP}	7	7	7	7	7	7
e_{HP}	0.67	0.67	0.67	0.67	0.67	0.67
ρ_{SA}	0	0	8	0	0	0
ρ_{HP}	0	0	0	0	30	0
ω_{SA}	0	0	2.1	0	0	0
ω_{HP}	0	0	0	0	0.8	0
k_{SA-AV}	3	0.66	0.66	3	3	3
k_{AV-HP}	55	14	14	45	30	14
k^{τ}_{SA-AV}	3	0.02	0.09	3	3	0.4
k^{τ}_{AV-HP}	55	60	38	20	30	38
τ_{SA-AV}	0.8	0.66	0.8	0.8	0.8	0.8
τ_{AV-HP}	0.1	0.1	0.1	0.1	0.1	0.1
β_t	0.1048	0.0809	0.0230	0.1111	0.1048	0.5283

3. Numerical simulations

The fourth order Runge-Kutta method with linear interpolation of time-delayed variables is used to integrate governing equations (2) [67]. In order to treat the DDEs system, it is necessary to approximate their solutions for time instants before τ_j. A Taylor series expansion is proposed [2,68].

$$x_i^{\tau} = x_i - \tau\left(\frac{x_{i+1} - x_i}{h}\right) \tag{6}$$

A convergence analysis reveals that time steps smaller than $h = 10^{-3}$ presents error of the order of 10^{-6}, considered satisfactory.

3.1. Cardiac system simulations

Numerical simulations of the cardiac system model are performed with the objective of presenting different system behaviors. The idea is to compare normal and pathological responses represented by ECGs. Experimental ECG data available on PhysioNet Databases [69] and Canabrava [70] are used as a reference. In all simulations the following parameters are used: $\beta_0 = 1$ mV, $\beta_1 = 0.06$ mV, $\beta_2 = 0.1$ mV, $\beta_3 = 0.3$ mV; and the following initial conditions are applied [63]:

$$\boldsymbol{x}_0 = \left[-0.1 \;\; 0.025 \;\; -0.6 \;\; 0.1 \;\; -3.3 \;\; \frac{10}{15}\right]^T \tag{7}$$

Six cases are investigated in order to evaluate the model capability to represent heart dynamics: normal rhythm, atrial flutter, atrial fibrillation, ventricular flutter and two different ventricular fibrillation cases, with and without external stimulus. The idea is to consider classical ECG patterns captured from the second derivation, associated with each one of these behaviors. It is important to highlight that variations of these patterns are possible due to person characteristics. Table 1 summarizes parameter values employed for simulations of different cardiac rhythms. Each case is treated in the sequence, highlighting the conceptual model of each one of them, elucidating the parameters presented in Table 1. Parameters that are null for all cases are omitted.

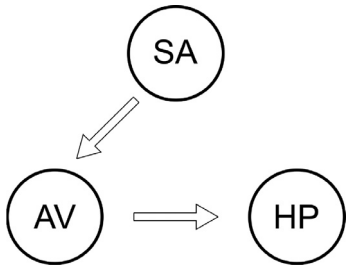

Fig. 3. Conceptual model of the normal heart functioning characterized by sinoatrial node (SA), atrioventricular node (AV) and His-Purkinje complex (HP) with symmetrical and unidirectional connections.

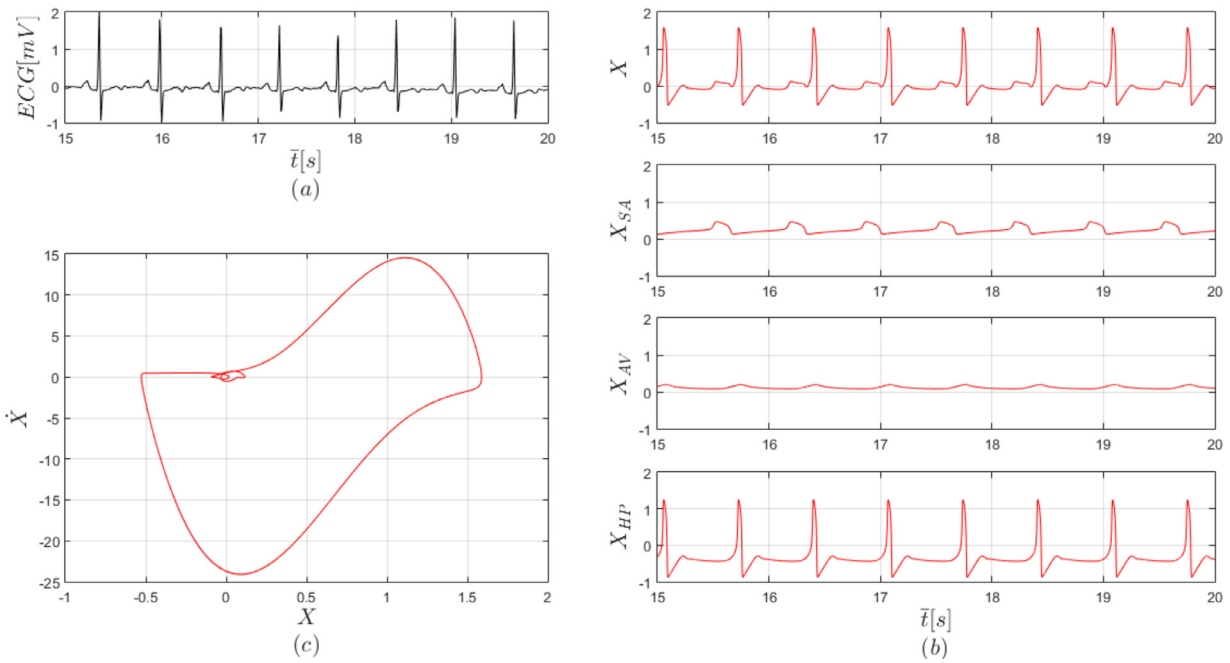

Fig. 4. Normal rhythm functioning by different perspectives: (a) experimental signal [69]; (b) simulated time series response of ECG signal (X) and each oscillator ($\boldsymbol{X_{SA}}$,$\boldsymbol{X_{AV}}$***and*** $\boldsymbol{X_{HP}}$); (c) state space represented by subspace $\{\boldsymbol{X}, \dot{\boldsymbol{X}}\}$.

3.1.1. Normal rhythm

Normal heart rhythm has unidirectional couplings in such a way that the electrical impulse is conducted from SA node to AV node and then, from AV node to HP complex. External stimulus does not exist. The conceptual model of this behavior is schematically represented in Fig. 3.

Fig. 4 presents results related to the normal functioning ECG. Fig. 4-a shows experimental data [69]. Fig. 4-b presents simulated normal ECG and each oscillator response that compose ECG response. Fig. 4-c presents state space represented by subspace $\{X, \dot{X}\}$. Note that simulations capture the main features of the experimental ECG, presenting P, QRS and T waves, being in close agreement with experimental data.

3.1.2. Atrial flutter

Atrial flutter is a rhythmic disorder classified as supraventricular tachycardia, an increasing in heart frequency, characterized by very high atrial rate, usually 300 bpm, ranging from 240 to 430 bpm [71]. According to the electrophysiological mechanism, flutter is classified into two types: type I (or typical) and type II (or atypical). Type I is characterized by a macro-circuit of reentry in the right atrium with counterclockwise (most common) or clockwise rotation, presenting an ECG with P-waves with "sawtooth" form, called *f* waves [70]. Atrial flutter of type II is also caused by a reentry macro-circuit, but does not present a defined pattern of rotation direction, being more complex [72].

Atrial flutter of type I is now of concern. Atrial flutter heart rate response depends on the refractory period of the AV node. Under normal conditions, AV node filters the atrial stimuli which means that if the AV nodule is half the atrial rate, the AV conduction is 2:1. Conceptual model is similar to the one employed to the normal ECG (Fig. 3), making parameter changes in order to increase self-excitation frequency of the SA oscillator. In addition, coupling term value between SA and

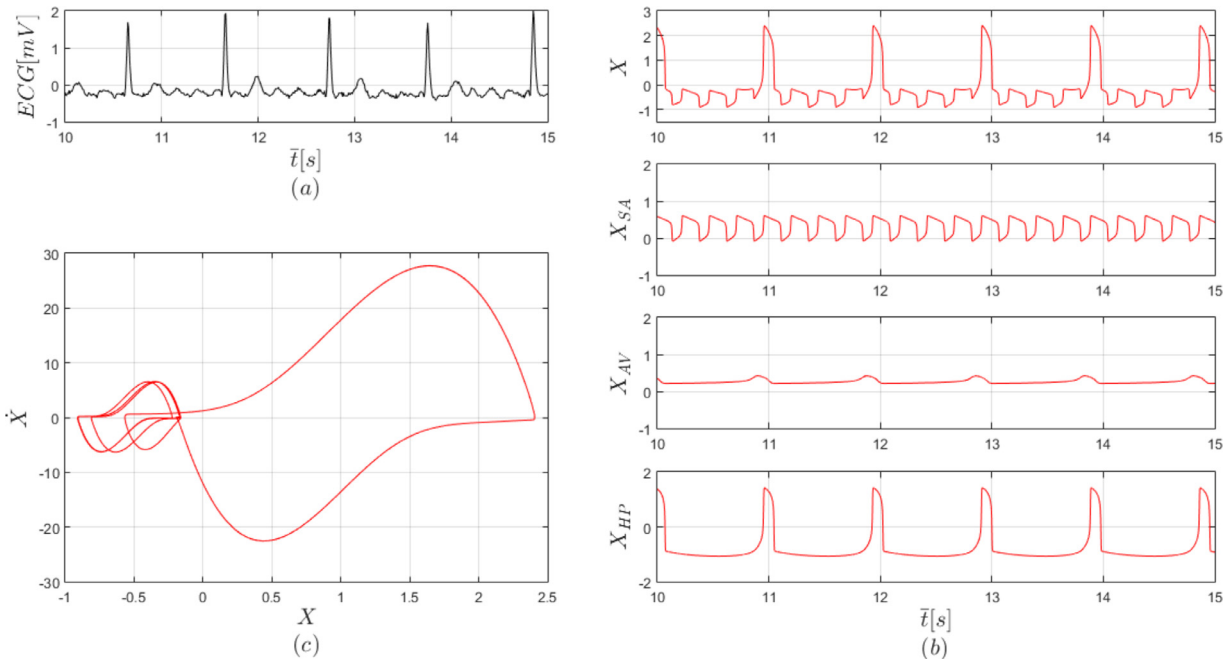

Fig. 5. Atrial flutter by different perspectives: (a) experimental data with 4:1 conduction [69]; (b) simulated time series response of ECG signal (X) and each oscillator ($\boldsymbol{X_{SA}}$,$\boldsymbol{X_{AV}}$ **and** $\boldsymbol{X_{HP}}$); (c) state space plot of subspace $\{\boldsymbol{X}, \dot{\boldsymbol{X}}\}$.

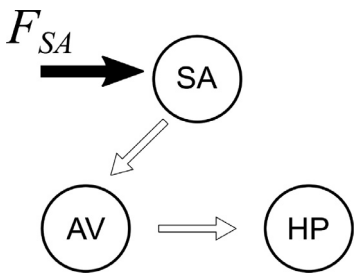

Fig. 6. Conceptual model of atrial fibrillation considering an external stimulus at the SA node.

AV oscillators is reduced representing the filtering behavior of the SA signal frequency (see Table 1). Fig. 5 presents different perspective of the atrial flutter including experimental data with 4:1 conduction (Fig. 5-a), numerical simulation time series for the ECG and each node signal (Fig. 5-b) and state space (Fig. 5-c). It is noticeable the good qualitative agreement between numerical and experimental results.

3.1.3. Atrial fibrillation

Atrial fibrillation is a pathological heart rhythm characterized to the existence of several atrial reentry circuits. These multiple circuits are formed at different times and locations in the atrial myocardium, leading to chaotic atrial contraction, with a frequency of 400 to 600 bpm [73]. This causes a non-effective atrial contraction, resulting in the formation of atrial thrombi that may break off and cause a cerebrovascular accident (CVA).

The AV node prevents these high-frequency stimuli to reach ventricles, promoting a filter that reduces frequencies to be from 90 to 170 bpm, avoiding ventricular fibrillation. Atrial fibrillation is characterized by an irregular R-R interval. In terms of mathematical model, the multiple ectopic foci may be represented by an SA node external stimulus. The conceptual model of this situation is shown in Fig. 6. In addition, proper couplings need to be considered as presented in Table 1.

Fig. 7 presents results related to the atrial fibrillation. Fig. 7-a shows experimental data where it is possible to highlight the irregular R-R interval. ECG numerical simulation is presented in Fig. 7-b together with each oscillator response. Fig. 7-c presents state space showing a dense region around the orbit of normal state space. It is noticeable that the model captures the general behavior of the experimental atrial fibrillation, presenting a R-R interval irregularity and the actuation of the AV node as a pacemaker.

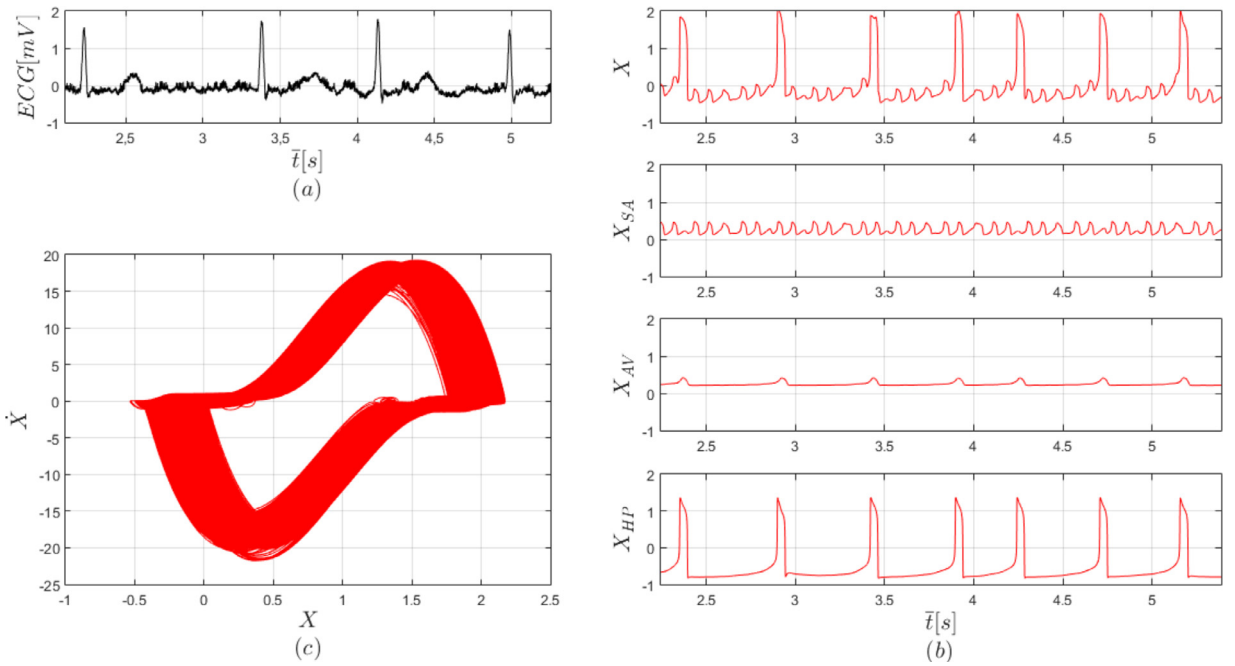

Fig. 7. Atrial fibrillation by different perspectives: (a) experimental signal [69]; (b) simulated time series response of ECG signal (X) and each oscillator ($\boldsymbol{X_{SA}}$,$\boldsymbol{X_{AV}}$***and*** $\boldsymbol{X_{HP}}$); (c) state space plot of subspace $\{\boldsymbol{X}, \dot{\boldsymbol{X}}\}$.

3.1.4. Ventricular flutter

Ventricular flutter is a tachycardia caused by a single ectopic focus or peripheral reentry mechanisms. Usually, it evolves to ventricular fibrillation, the most dangerous pathological heart rhythm. High frequency ventricular contraction (300 bpm) causes changes in muscle tissue stiffness in different cell groups, reflecting differences on the stimuli conduction velocity. Thus, multiple ventricular outbreaks are activated, establishing the fibrillatory process [74].

Flutter are usually caused by chronic processes (hypertensive, atherosclerotic, rheumatic), but can be induced by acute myocardial infarction that end up seriously heart compromising. Typically, ventricular flutter ECG is characterized to present the QRS complex, the S-T segment and the T wave incorporated into a single bell large-wave form, differing from the atrial flutter *f* waves.

Ventricular flutter conceptual model is the same of the one employed to describe atrial flutter (Fig. 3). Nevertheless, in order to obtain the effect of a ventricular ectopic focus, HP complex oscillator parameters are changed, keeping the other oscillator parameters equal to the normal case. Fig. 8 presents ventricular flutter results. Fig. 8-a shows an experimental response. Once again, numerical results presented in Fig. 8-b capture the general experimental behavior, presenting an ECG with similar characteristics. Numerical state space is presented in Fig. 8-c where it is possible to observe an enlargement of orbits around the greater loop of normal response.

3.1.5. Ventricular fibrillation

Ventricular fibrillation is a disordered myocardial contraction due to the chaotic activity of several ectopic foci located in the ventricles. This behavior results in total heart pumping inefficiency and, from the hemodynamic point of view, corresponds to cardiac arrest [74]. The causes of ventricular fibrillation are similar to the ones of ventricular flutter: Purkinje ventricular fibers produce irregular electrical distribution that characterizes irregular tracing in which P waves, QRS complex and T waves are not recognized. There are several variations of ventricular fibrillation ECGs and some possibilities are shown in Fig. 9.

There are different possibilities for the mathematical description of the ventricular fibrillation. Here, two alternatives are treated: the first one uses a conceptual model presented in Fig. 10, similar to the one employed to represent atrial fibrillation, but applying the external stimulus on the HP oscillator in order to represent multiple ectopic foci stimulation. The second approach represents ventricular fibrillation without external stimulus, considering a conceptual model similar to the normal one.

In this regard, ventricular fibrillation is now of concern considering two cases: with external stimulus (Figs. 11) and without external stimulus (Figs. 12). Fig. 11-a shows experimental data. Fig. 11-b shows ECG and individual oscillator time series with external stimulus. Note that simulated results represent the irregular behavior of the ventricular fibrillation, being in agreement with the experimental ECGs. State space is presented in Fig. 11-c, where a filled space indicating a chaotic-like response.

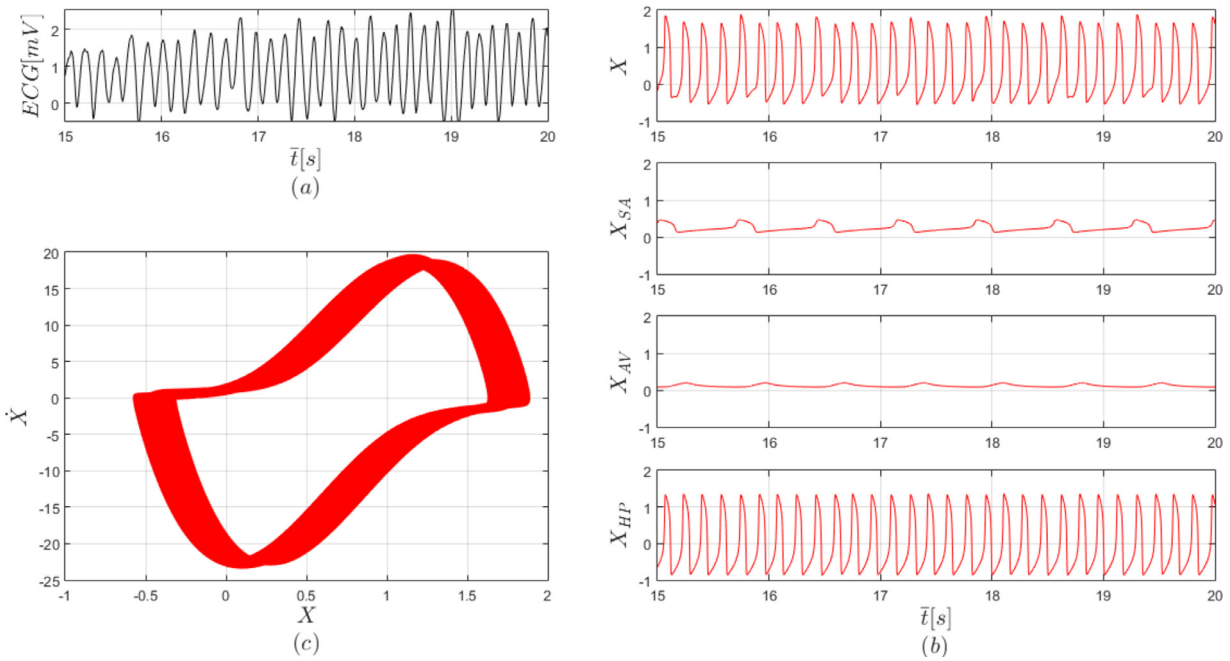

Fig. 8. Ventricular flutter by different perspectives: (a) experimental signal [69]; (b) simulated time series response of ECG signal (X) and each oscillator (X_{SA}, X_{AV} and X_{HP}); (c) state space plot of subspace $\{X, \dot{X}\}$.

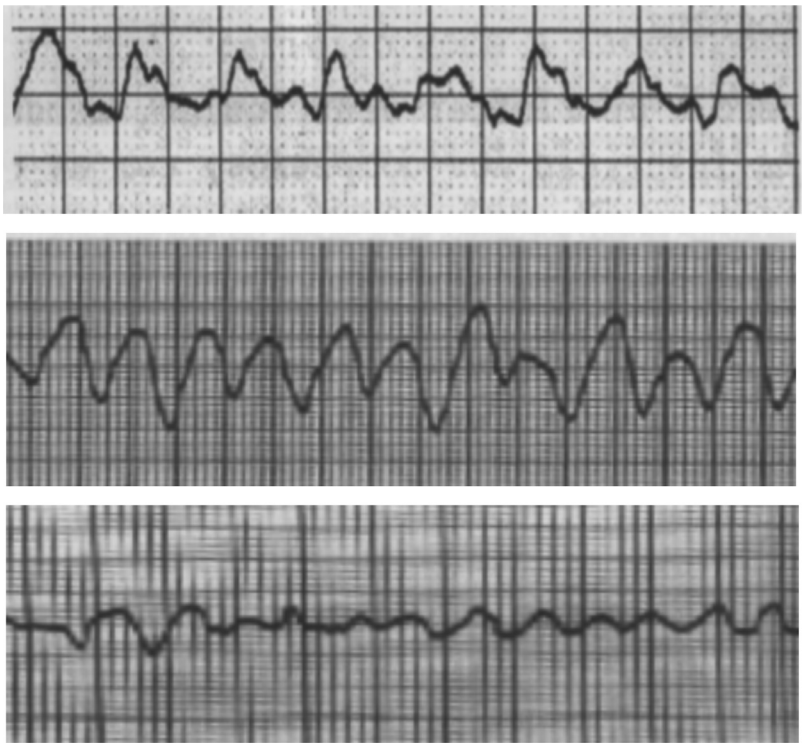

Fig. 9. Different ventricular fibrillation experimental ECGs [70] characterized by irregular electrical distribution with irregular tracing in which P waves, QRS complex and T waves are not recognized.

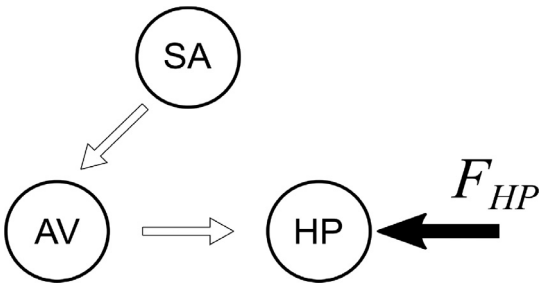

Fig. 10. Ventricular fibrillation conceptual model with external stimulus.

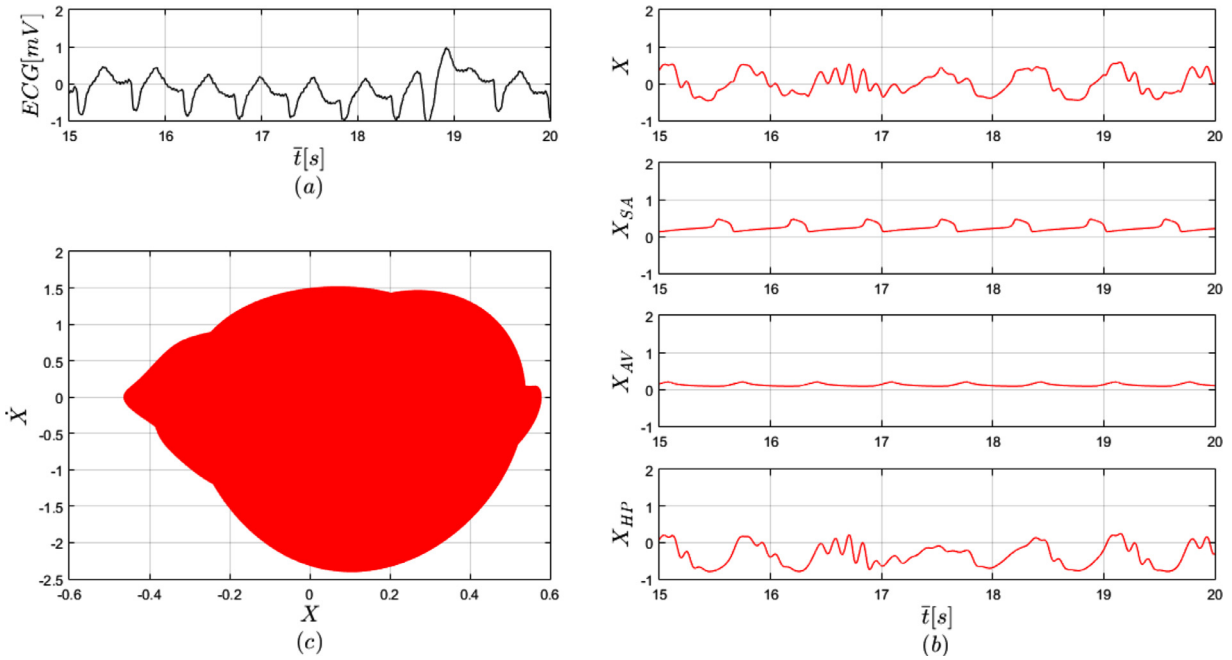

Fig. 11. Ventricular fibrillation with external stimulus: (a) experimental signal [69]; (b) simulated time series response with external stimulus of ECG signal (X) and each oscillator (X_{SA},X_{AV} and X_{HP}); (c) state space plot of subspace $\{X, \dot{X}\}$.

Another possibility to represent ventricular fibrillation is considering a conceptual model similar to the normal one, without external stimulus (Fig. 12). The effect of multiple ectopic foci is now represented by different coupling parameters (see Table 1). Fig. 12-a shows experimental data while Fig. 12-b presents simulations related to ECG and each oscillator time evolution. Once again, a filled chaotic-like state space is shown in Fig. 12-c.

4. Poincaré map

Poincaré map is a stroboscopic representation of the dynamical system response. It reduces the time continuous dynamics to a discrete set of states, a map, allowing a better understanding of the global system dynamics. There are different ways to build a Poincaré map and two approaches are employed in this work: return map and reference period.

Dynamics perspective is an interesting approach to identify heart rhythms and, in this regard, the kind of dynamical response is a valuable information. Lyapunov exponents are important to be estimated in order to identify chaotic response of cardiac systems. The time-delayed states dependence requires an appropriate approach for calculating the Lyapunov exponents. The same procedure considered by [62] is adopted in this work and it is concluded that normal and flutter (atrial and ventricular) are quasiperiodic responses while fibrillation (atrial and ventricular) is a chaotic response.

4.1. Return map

Return map uses a geometrical inspiration to build Poincaré map considering successive trajectory intersections with a subsapace hypersurface. Fig. 13 shows a schematic picture of the use of a secant plane to build a Poincaré return map on

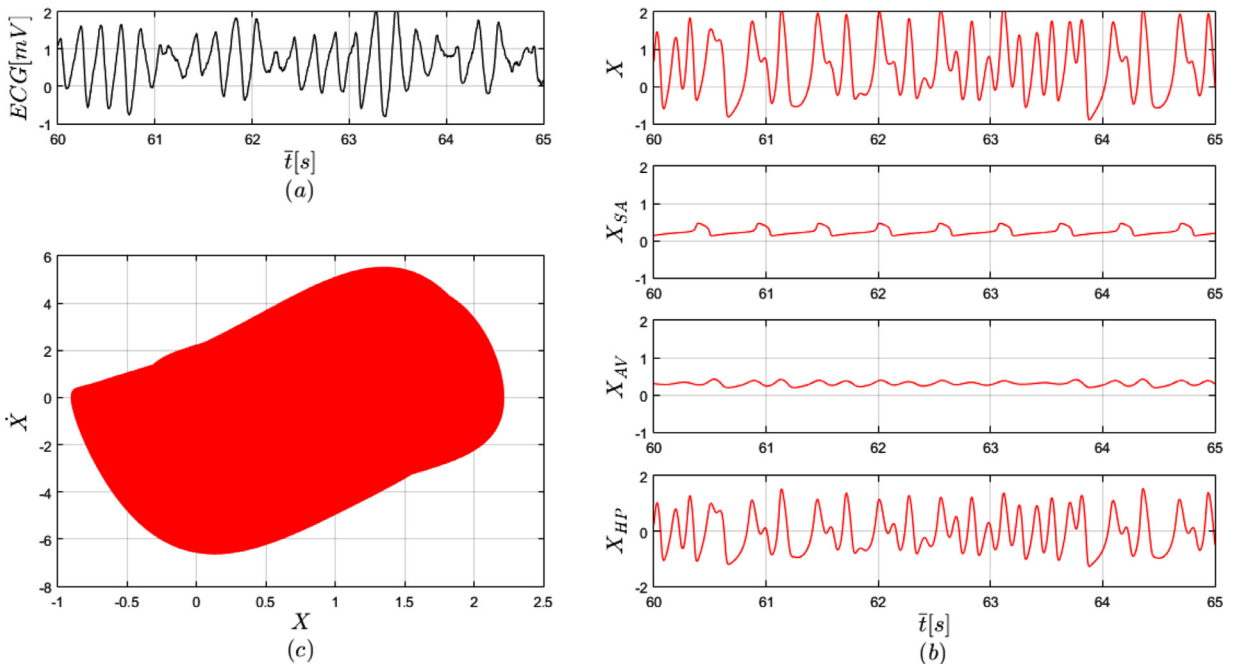

Fig. 12. Ventricular fibrillation without external stimulus: (a) experimental signal [69]; (b) simulated time series response without external stimulus of ECG signal (X) and each oscillator (X_{SA},X_{AV} and X_{HP}); (c) state space plot of subspace $\{X, \dot{X}\}$.

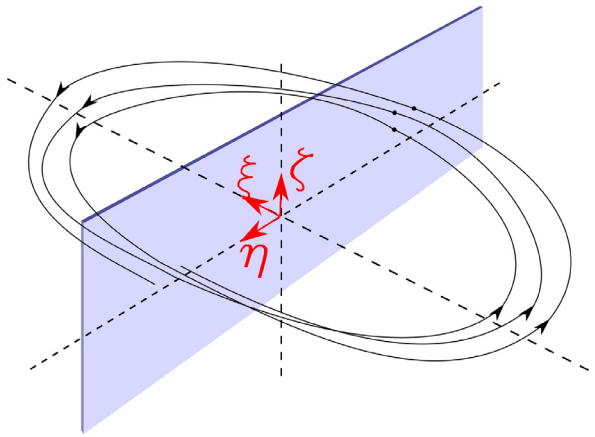

Fig. 13. Schematic picture of the Poincaré return map construction using a secant section. The map points are related to the vector field that transversally crosses a specific section in the positive direction of ξ, defining a state space subspace.

state space. Basically, map points are related to the vector field that transversally crosses a specific section in the positive direction of ξ, defining a state space subspace.

Heart dynamics analysis considers a subspace $\{x_1, X, \dot{X}\}$ where it is positioned a secant section according to the following equation, allowing the observation of states that crosses the section in the positive direction of x_1. A suitable Poincaré map is chosen in order to be representative through the system dynamic changes. Several coefficients of $\{x_1, X, \dot{X}\}$ were tested and the equation that best captured information about the system is presented in the sequence

$$x_1 + \frac{6}{4}X - 3\dot{X} + 3 = 0 \tag{8}$$

Fig. 14 presents different cardiac rhythms discussed in the previous section: normal rhythm; atrial flutter; atrial fibrillation; ventricular flutter; ventricular fibrillation with and without external stimulus. System trajectory in blue, the Poincaré section, represented by the gray plane, and the projections of system trajectory in black and of Poincaré map in red. It is noticeable that Poincaré maps furnish a different system dynamics perspective and this can be employed for identification purposes.

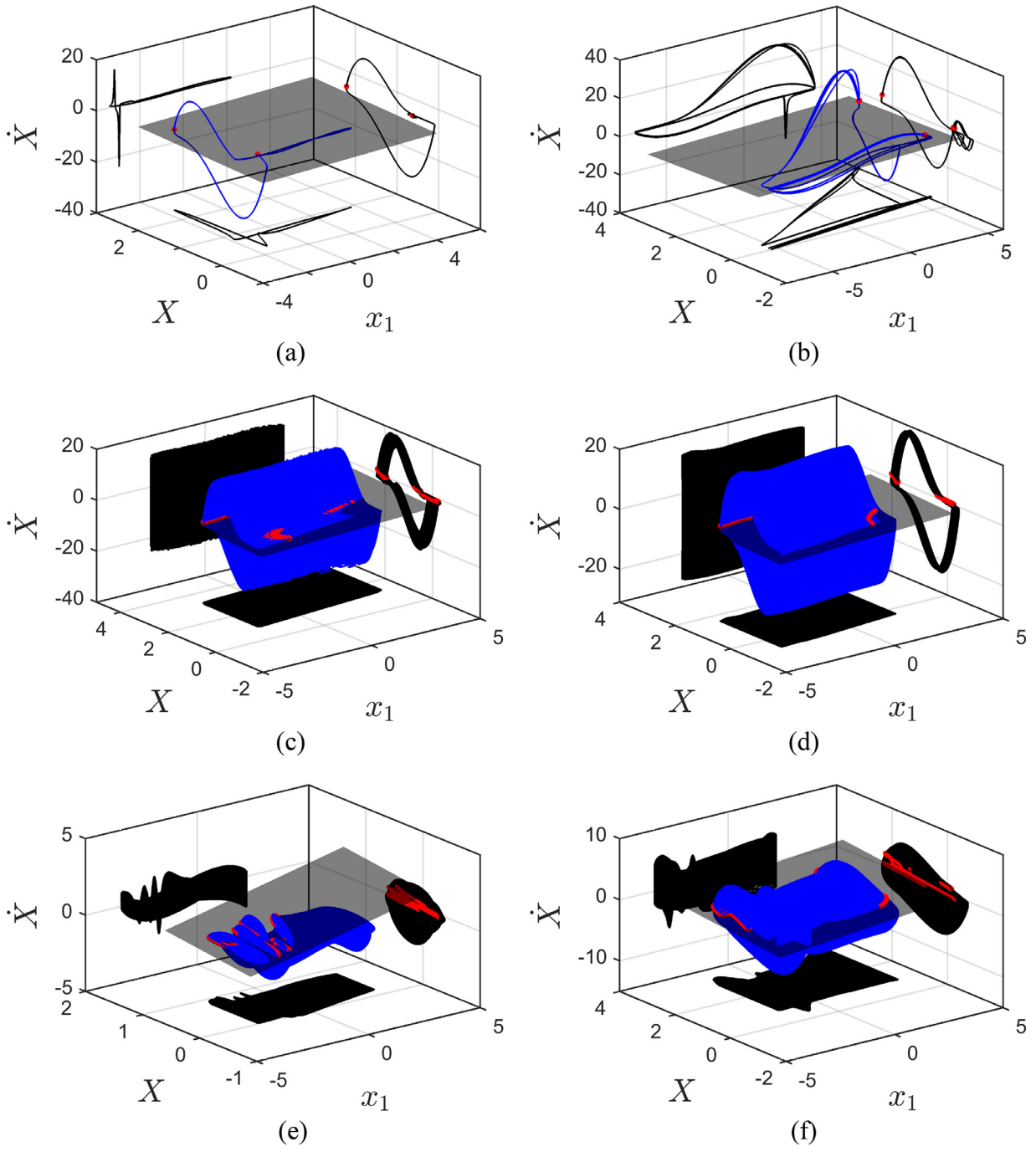

Fig. 14. Poincaré sections built with a secant section approach. (a) Normal rhythm; (b) atrial flutter; (c) atrial fibrillation; (d) ventricular flutter; (e) ventricular fibrillation with external stimulus; (f) ventricular fibrillation without external stimulus.

Fig. 15 presents an overlap of all the Poincaré maps in $A - B$ plane, allowing a comparative analysis among different rhythms. In general, it is possible to identify the main differences from the normal rhythm, considered as the system signature reference. Normal rhythm is characterized by a map containing two points (black). Atrial flutter has three clusters of points (purple). Ventricular flutter map covers one straight line and one closed curve (yellow). Ventricular fibrillation without external stimulus shows a map (green) with a discontinuous structure. This same kind of behavior is observed in the ventricular fibrillation with external stimulus (blue). Atrial fibrillation map (red) also shows a discontinuous structure, with higher irregularity. This analysis suggests that critical pathological behaviors are distinguishable using Poincaré maps.

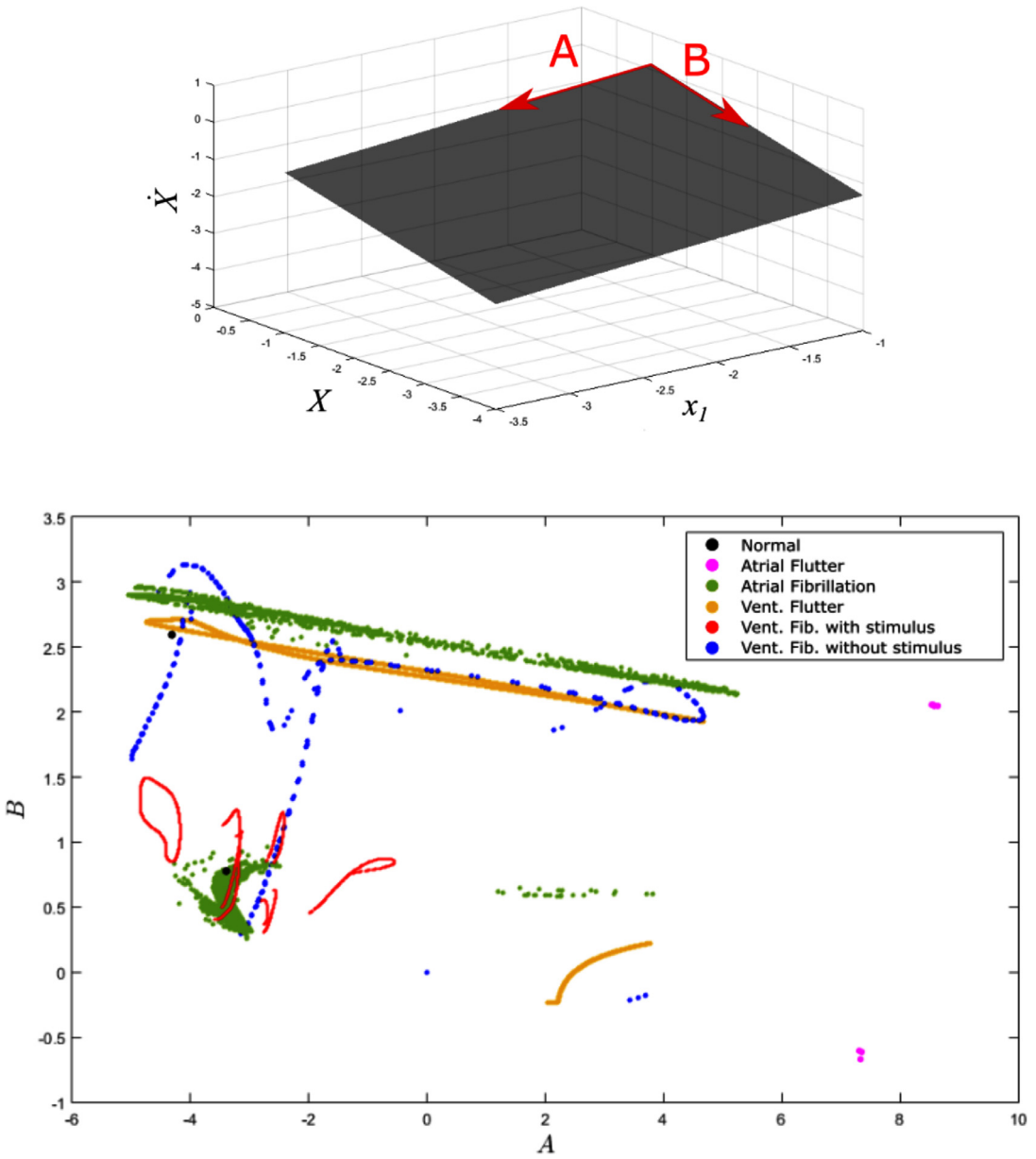

Fig. 15. Projections $\boldsymbol{A} - \boldsymbol{B}$ of Poincaré maps built with secant section for different heart rhythms associated with different patterns.

4.2. Reference period map

Poincaré map can be built by considering a reference period that defines the stroboscopic sample time. This procedure establishes the section position spaced by a period T through time, observing system dynamics states through the section, as presented in schematic picture of Fig. 16. A straightforward approach to define reference period is when the system is subjected to a harmonic excitation, and the excitation frequency defines the reference period. Otherwise, it is necessary to define a proper reference period, a self-excitation period. The self-excitation period of the heart rhythm can be analyzed from the R-R interval measurement. In this regard, a histogram of the R-R interval is built, establishing the mean value, , that defines the reference period for the Poincaré map construction.

In the sequence, this procedure is applied to evaluate system dynamics considering results, as function of dimensionless time, discussed in the preceding sections. Note that atrial fibrillation and ventricular fibrillation with external stimulus are built using external excitation period; the other rhythms use the self-excitation period. Fig. 17 presents R-R interval histogram for the cases without external stimulus: normal rhythm, atrial flutter, ventricular flutter and ventricular fibrillation without external stimulus. Based on this analysis, it is possible to establish a mean value of each case that is employed to

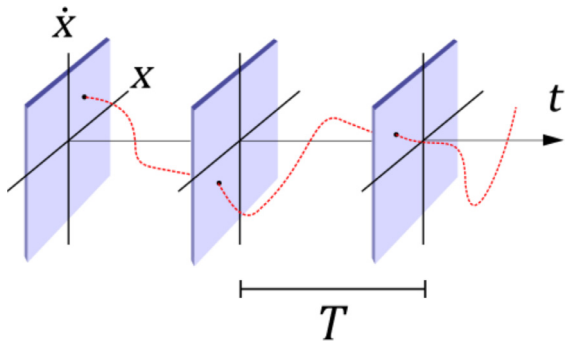

Fig. 16. Schematic picture of Poincaré map built using a reference period that defines the stroboscopic sample time.

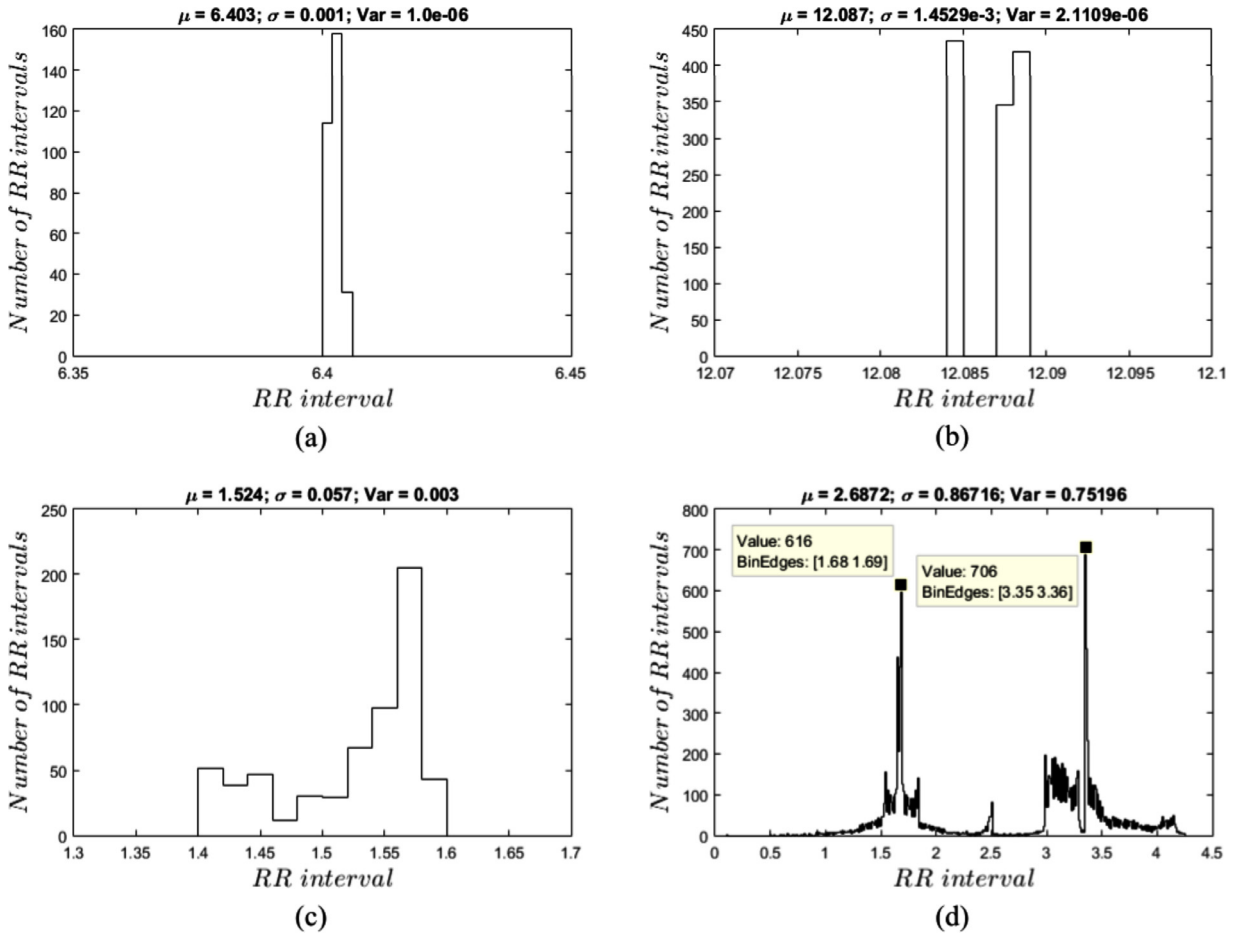

Fig. 17. R-R interval histogram for different cardiac rhythms. (a) Normal rhythm; (b) atrial flutter; (c) ventricular flutter; (d) ventricular fibrillation without external stimulus.

define the self-excitation period. Table 2 presents mean values of each one of the cases. By considering the ventricular fibrillation without external stimulus, it should be pointed out that there are two peaks 1.68 and 3.35 that can suggest another reference period.

Fig. 18 presents Poincaré maps for all the cases, built with the appropriate procedure. It is again important to observe that Poincaré map is an interesting approach to identify the kind of response. It should be pointed out that ventricular fibrillation without external stimulus has other possibilities due to a two-peak R-R interval histogram. Fig. 19 presents the three possibilities, showing that they are similar.

Fig. 20 presents a comparative analysis of all rhythms using Poincaré maps built with reference period. Once again, it is possible to identify variations of pathological responses from the normal rhythm. Normal rhythm is not characterized

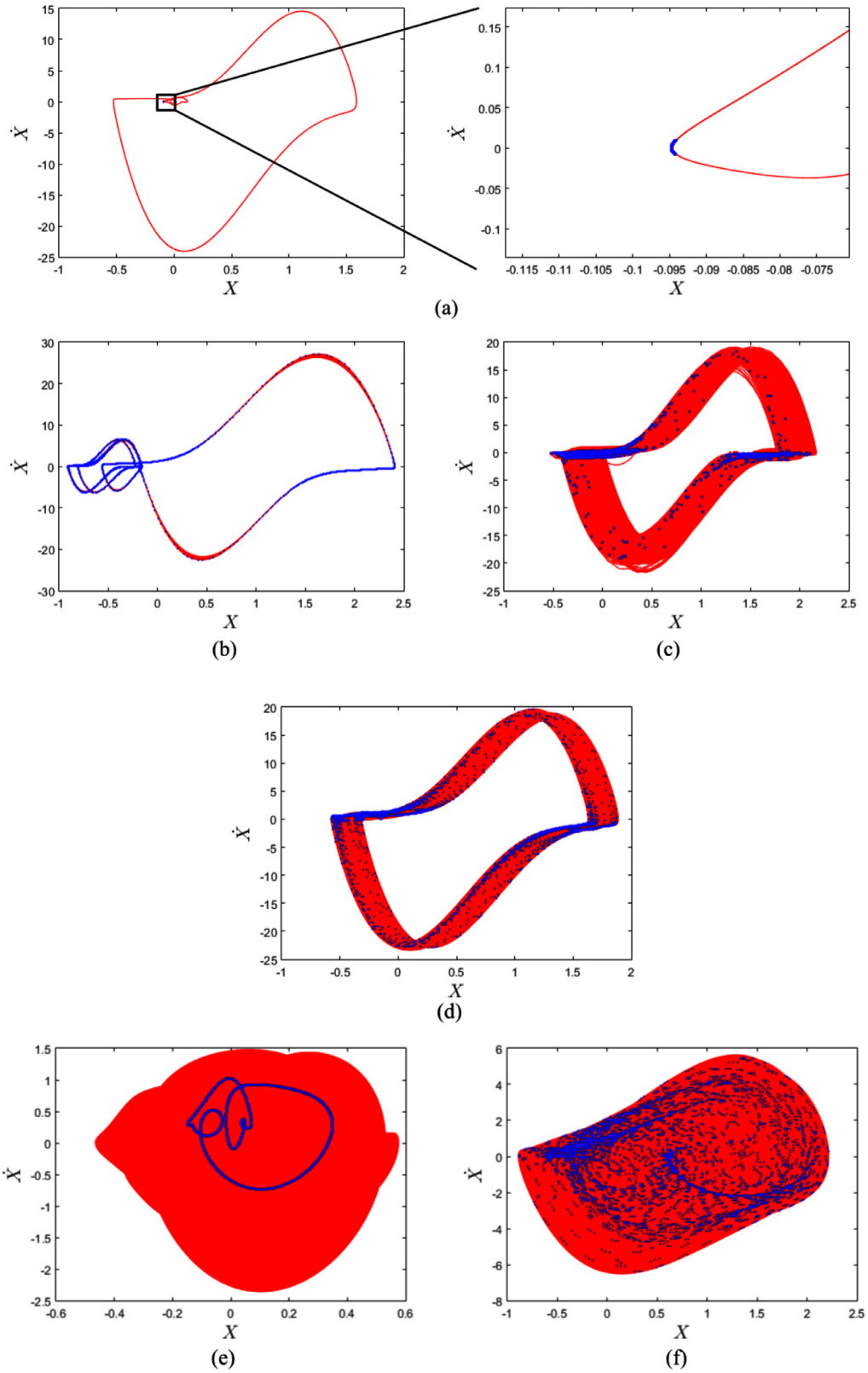

Fig. 18. Poincaré sections (blue) built with reference period. (a) Normal rhythm; (b) atrial flutter; (c) atrial fibrillation; (d) ventricular flutter; (e) ventricular fibrillation with external stimulus; (f) ventricular fibrillation without external stimulus.

Table 2
Mean values employed as self-excitation period that defines Poincaré map period.

Heart rhythm	Mean value (μ)
Normal rhythm	6.403
Atrial flutter	12.067
Ventricular flutter	1.524
Ventricular fibrillation without external stimulus	2.67

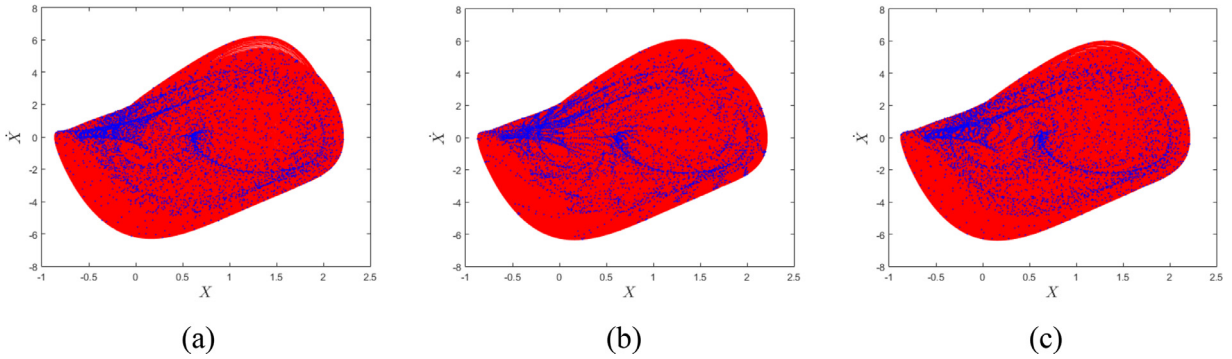

Fig. 19. Ventricular fibrillation without external stimulus ECG state space (red) and Poincare maps (blue) built with the following reference period: (a) $T = 1.68$; (b) $T = 2.67$ and (c) $T = 3.35$.

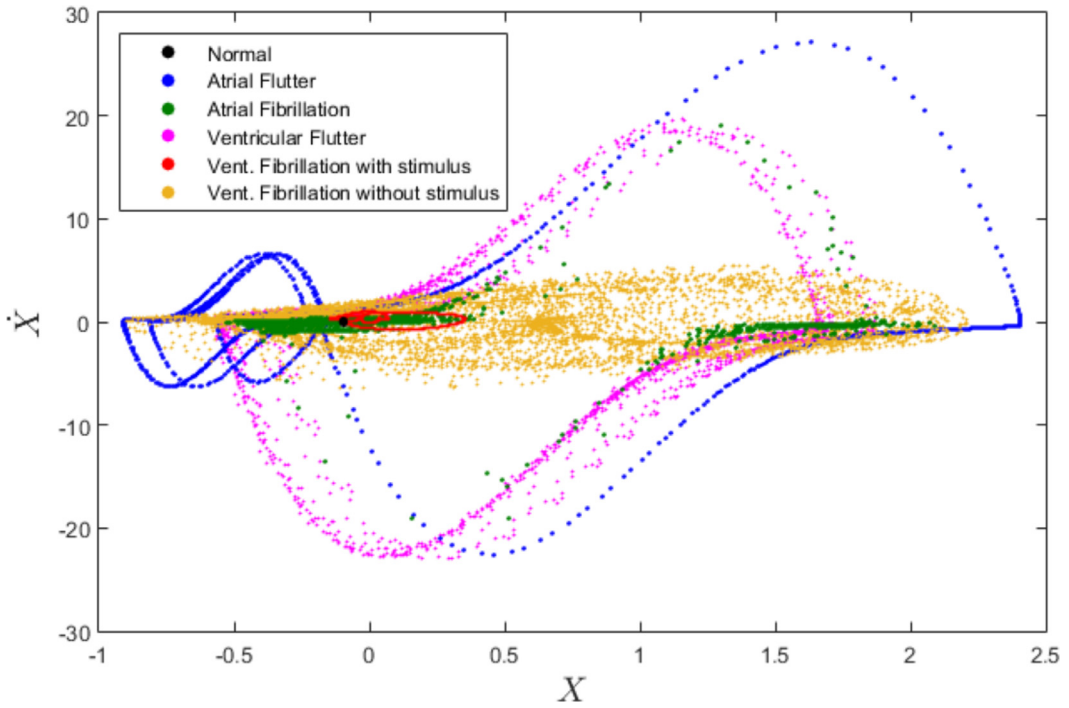

Fig. 20. Comparison of Poincaré maps built with reference period for different rhythms.

by a point, but as a small neighbor (black). Atrial flutter (yellow) and ventricular flutter (purple) maps are closed curves with different amplitudes, representing a quasi-periodic behavior. Atrial fibrillation shows a chaotic-like map with two distinguishable clouds of points (green). Ventricular fibrillation with external stimulus has a closed curve map, with smaller amplitude compared with the previous cases (red). Ventricular fibrillation without external stimulus shows a chaotic-like attractor map (blue). Results allow one to obtain similar conclusions with the ones with the other Poincaré map construction but point that different alternatives can be imagined to build Poincaré maps.

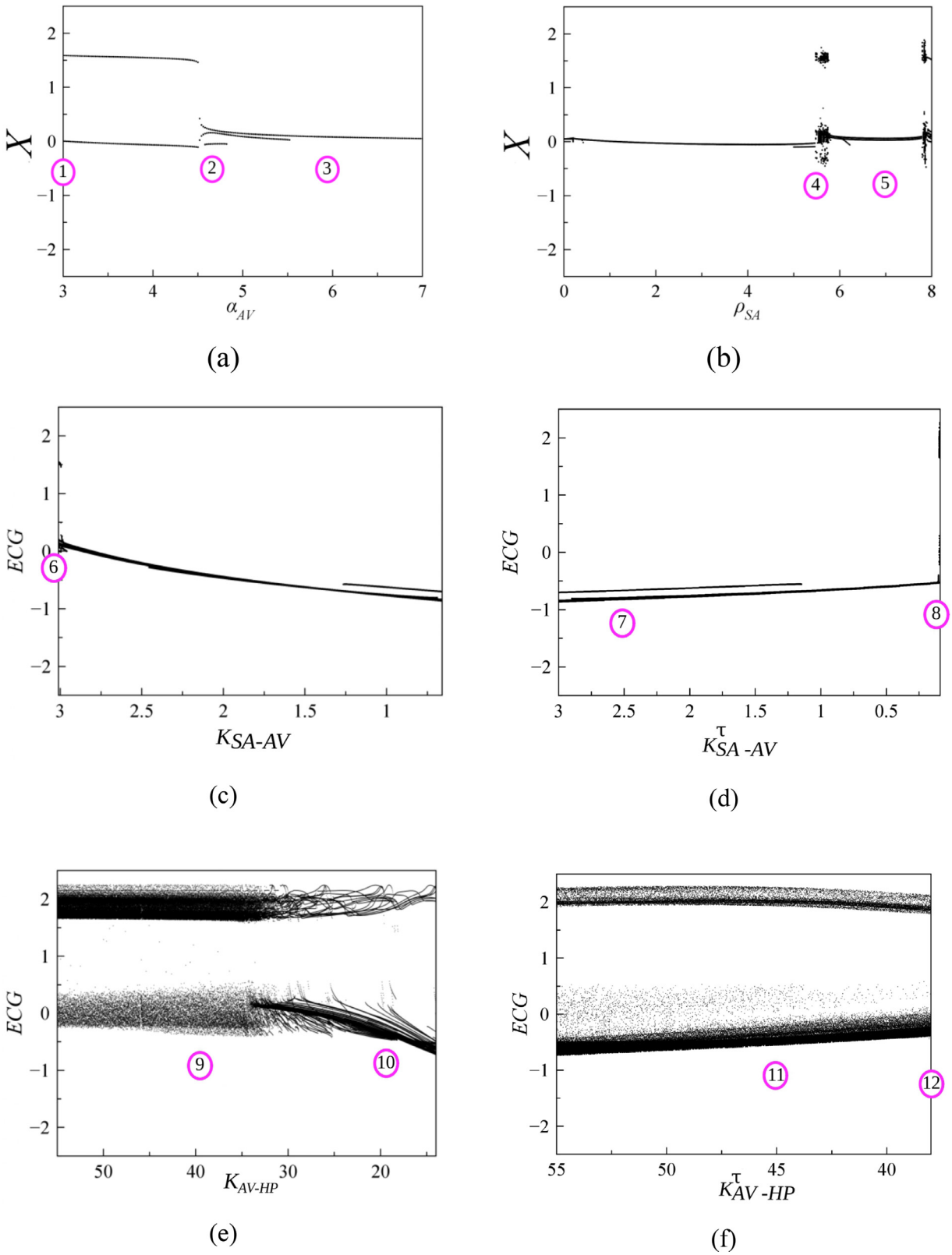

Fig. 21. Bifurcation diagrams establishing the route from normal functioning to atrial fibrillation varying α_{AV}, ρ_{SA}, ω_{SA}, k_{SA-AV}, k^{τ}_{SA-AV}, k_{AV-HP} and k^{τ}_{AV-HP} in an independent way. Regions 1, 2 and 3 present quasi-periodic behaviors. Regions 4 and 6 present more complex behaviors. Region 7 is related to quasi-periodic behavior. Region 8 indicates the beginning of a more complex behavior presented in regions 9, 10 and 11. Region 12 is related to the atrial fibrillation response.

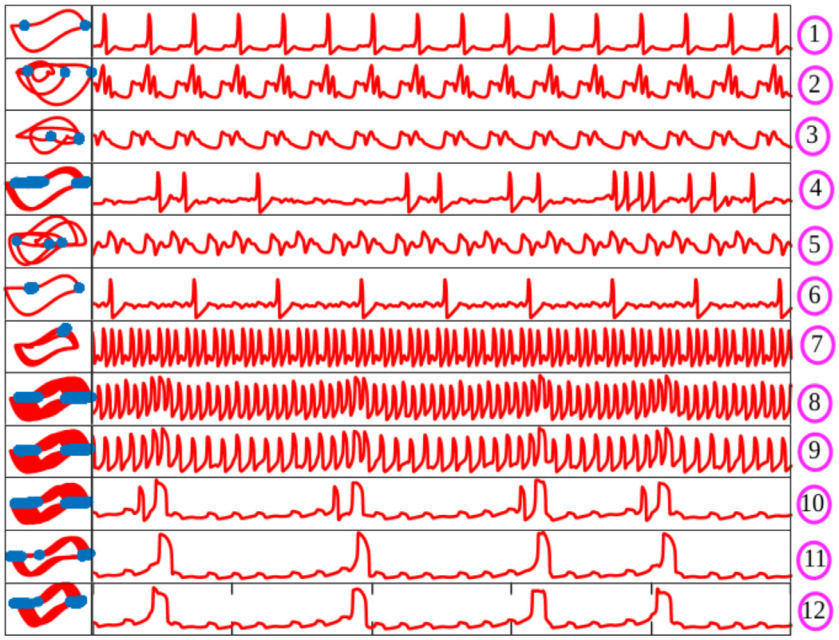

Fig. 22. Responses defining the routes from normal functioning to atrial fibrillation, being associated with different regions of the bifurcation diagrams represented by ECG evolutions, phase space and Poincaré maps.

5. Bifurcation analysis

This section has the goal to investigate the route from normal functioning to pathologies. In this regard, bifurcation analysis is carried out defining parameter variations. One parameter is varied at a time and each parameter variation corresponds to a different bifurcation diagram. Bifurcation diagrams are built by the ECG response using the Poincaré return map defined in Eq. (8). For each parameter, the system is integrated 600 s and the first 250 s are neglected in order to reach steady state responses. Three routes are treated, by considering normal functioning to fibrillation (atrial and ventricular with and without stimulus), which is a typical chaotic response.

It should be pointed out that each parameter is varied, independently from the others, evaluating one solution from each variation. Based on that, only one stable solution is shown per one set of parameter values, without analyzing coexisting solutions. This means that the route from normal to pathological behaviors is evaluated. Other possible routes can exist together with the ones discussed.

5.1. Bifurcation from normal functioning to atrial fibrillation

This section considers the route from normal functioning to atrial fibrillation. An analysis of the system parameters presented in Table 1 shows that seven of them are different when comparing normal functioning and atrial fibrillation: α_{AV}, ρ_{SA}, ω_{SA}, k_{SA-AV}, k^{τ}_{SA-AV}, k_{AV-HP} and k^{τ}_{AV-HP}. Fig. 21 presents the bifurcation diagram starting with the set of parameters related to the normal functioning and finishing with the set of parameters related to the atrial fibrillation, varying each one in an independent way, following the sequence presented. Dynamical changes are pointed in the bifurcation diagrams by regions, identified by numbers circled with magenta. Each parameter is altered until it reaches the corresponding value of the atrial fibrillation. Although seven parameters are modified, only six of them are varied as shown in the six bifurcation diagrams presented in Fig. 21. The external stimulus has two parameters associated with: forcing amplitude and frequency. When forcing amplitude ρ_{SA} variation is performed, the forcing frequency, ω_{SA}, is assumed to be constant. Thus, there is no bifurcation diagram associated to ω_{SA}, as when it is considered it assumes a constant value. Fig. 21-a shows the variation of α_{AV}, being related to regions 1, 2 and 3 that present quasi-periodic behaviors. Fig. 21-b varies ρ_{SA} while a constant value of $\omega_{SA} = 2.11$ is considered, defining regions 4 and 5 with a more complex behavior. Fig. 21-c is related to region 6 due to the variation of k_{SA-AV}. The sequence establishes the variation of parameter k^{τ}_{SA-AV}, Fig. 21-d, defining regions 7 and 8 with the same characteristics of the previous Figure. Fig. 21-e establishes the variation of parameter k_{AV-HP} defining regions 9 and 10 with more complex behaviors. Finally, Fig. 21-e considers the variation of parameter k^{τ}_{AV-HP} following the same trends, defining regions 11 and 12 and the last region is related to the atrial fibrillation response.

Fig. 22 presents the heart dynamics showing the ECG, phase space and Poincaré section associated with each one of the previous regions. Responses related to regions 1 to 3 are quasi-periodic behaviors but with different characteristics. Responses of region 4 show more degenerate situations with a large variation of RR intervals. Response 5 shows an apparent

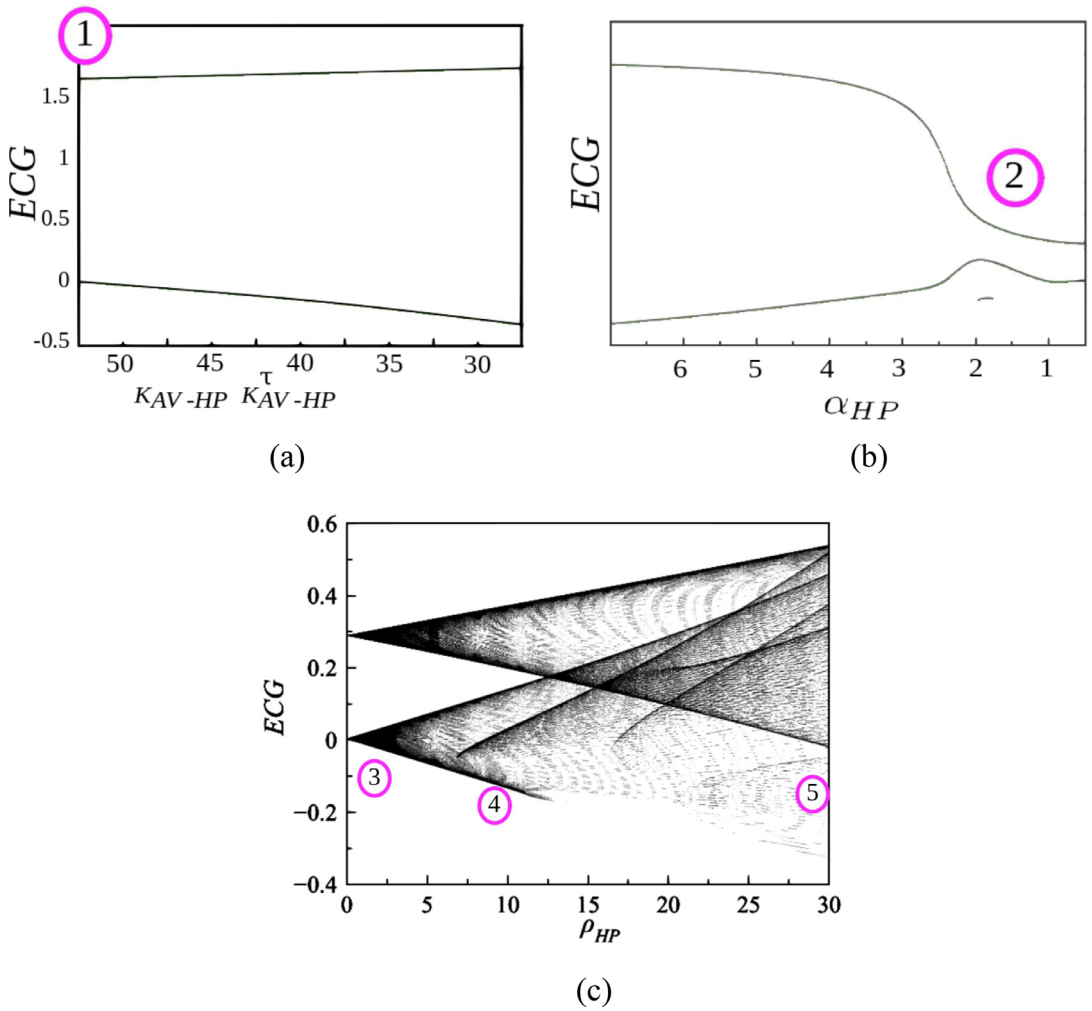

Fig. 23. Bifurcation diagram establishing the route from normal functioning to ventricular fibrillation with external stimulus varying paramerters k_{AV-HP}, k^{τ}_{AV-HP}, α_{HP}, ρ_{HP} and ω_{HP} in an independent way. Regions 1 and 2 present quasi-periodic responses. Regions 3–5 show a set of bifurcations that lead to ventricular fibrillation.

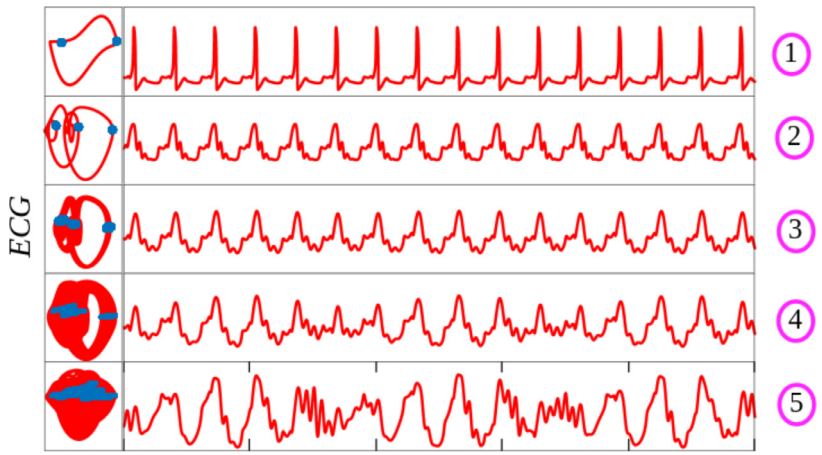

Fig. 24. Responses defining the routes from normal functioning to ventricular fibrillation with external stimulus, being associated with different regions of the bifurcation diagrams represented by ECG evolutions, phase space and Poincaré map.

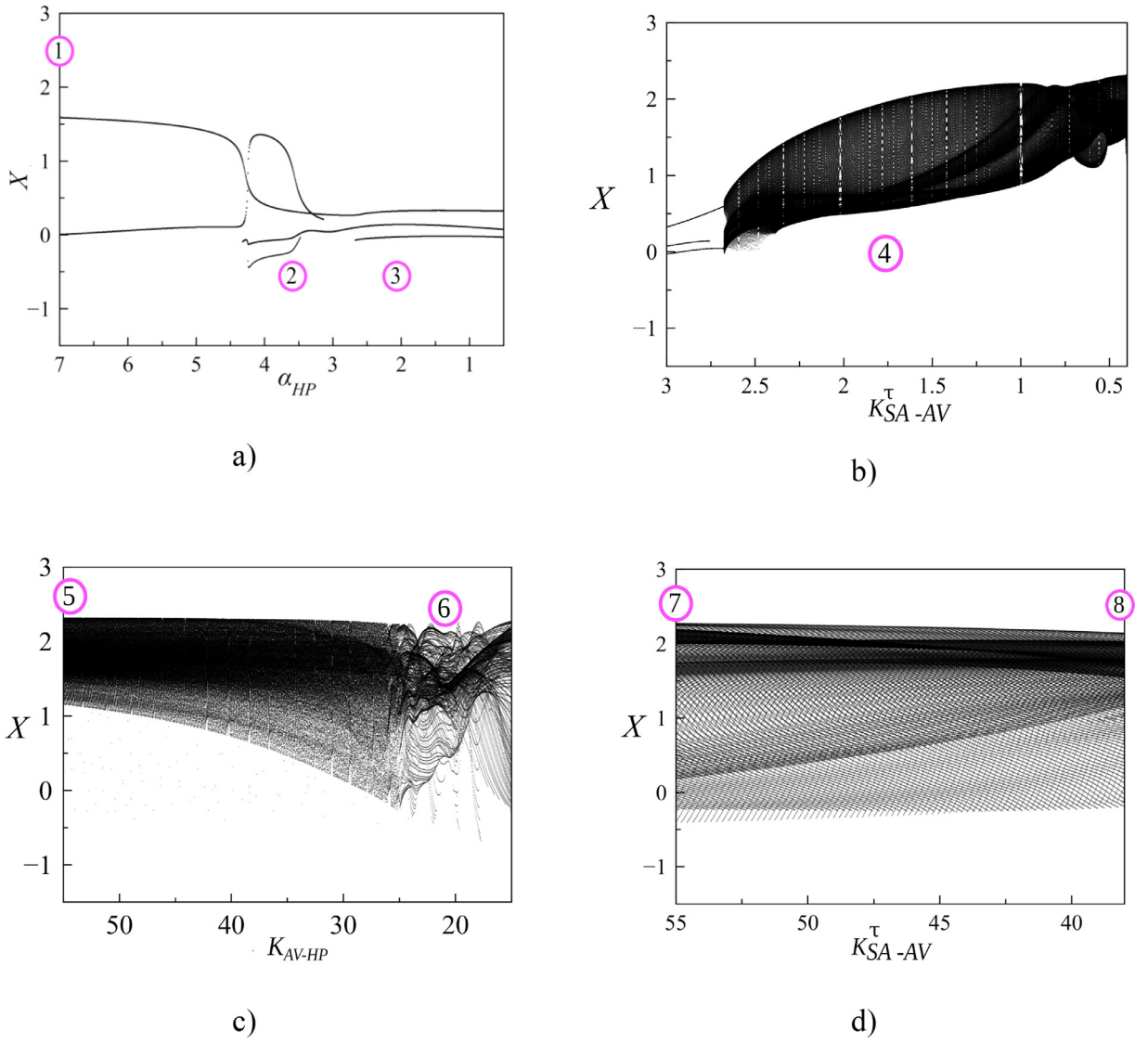

Fig. 25. Bifurcation diagram establishing the route from normal functioning to ventricular fibrillation without external stimulus varying parameters α_{HP}, k_{SA-AV}, $k_{AV-HP}$and k^{τ}_{AV-HP}in an independent way. Regions 1, 2 and 3 present quasi-periodic responses. Regions 4 and 5 present irregular behaviors with high beating frequency. Regions 6 show an evolution of a non-periodic complex behavior that lead to Ventricular fibrillation in regions 7–8.

periodicity while response 6 has similarities with the atrial fibrillation, with a QRS complex with variations in the beats related with the atria (see Fig. 7a). Responses 7 to 9 are similar, but with different Poincaré maps. Response 10 has a different ECG when compared to region 9, but with similar phase space and Poincaré map. Responses 11 and 12 present similar ECG and slight differences in Poincaré maps and phase spaces.

5.2. Bifurcation from normal functioning to ventricular fibrillation

The bifurcation from normal functioning to ventricular fibrillation is now in focus considering the same methodology of the previous section. Initially, the case with external stimulus is considered followed by the case without external stimulus.

5.2.1. Ventricular fibrillation with external stimulus

Ventricular fibrillation with external stimulus analysis is reached by variations of the parameters k_{AV-HP}, k^{τ}_{AV-HP}, α_{HP}, ρ_{HP} and ω_{HP}, with respect to normal functioning (Table 1). Fig. 23a presents bifurcation diagrams varying the coupling terms k_{AV-HP} and k^{τ}_{AV-HP} and since the coupling terms are identical, they are varied concomitantly. These variations define region 1 with quasi-periodic response. Fig. 23b presents bifurcation with parameter α_{HP} defining region 2 with the same

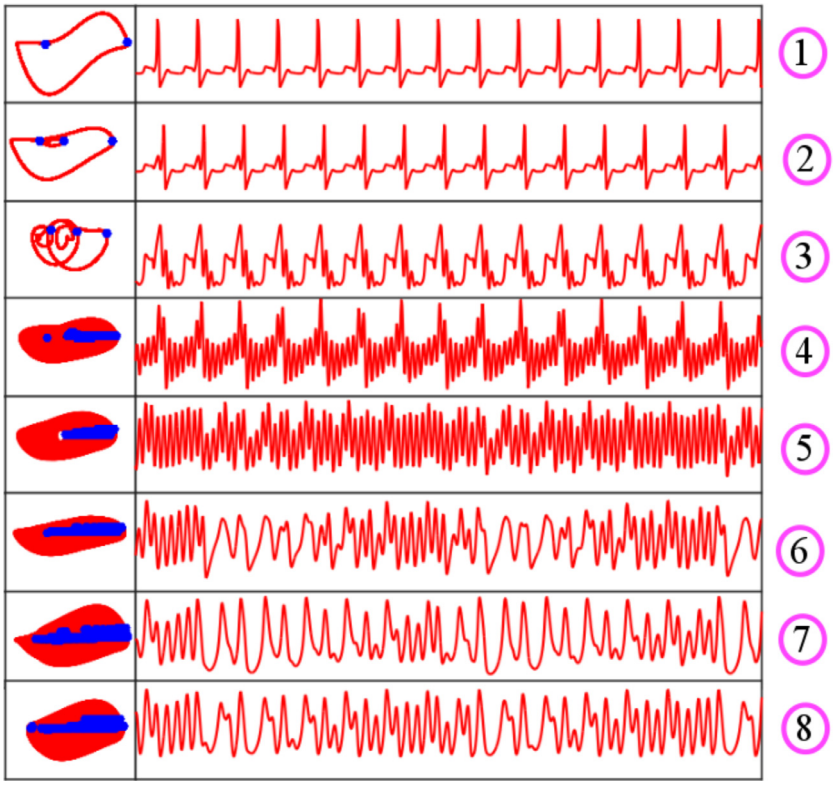

Fig. 26. Responses defining the routes from normal functioning to ventricular fibrillation without external stimulus, being associated with different regions of the bifurcation diagrams represented by ECG evolutions, phase space and Poincaré maps.

trend but showing an amplitude reduction. Afterward, variation on forcing parameters is performed. The forcing frequency is considered constant, $\omega_{HP} = 0.8$, while the forcing amplitude is increased, Fig. 23-c, defining regions 3, 4 and 5. These regions present a set of bifurcations that lead to ventricular fibrillation pathology.

Fig. 24 presents heart responses for each one of the regions discussed, showing ECG, phase space and Poincaré maps. Region 1 is related to the normal functioning evolving to region 2 that shows a high discrepancy of the normal ECG, where P and T waves are not detectable, presenting an overlap of the waves. Region 3 does not present a substantial difference when compared with the region 2, the difference appears in Poincaré section and phase space, as system visits a larger region. Region 4 has a more irregular ECG behavior. On the other hand, region 5 is related to the ventricular fibrillation and the response is related to the appearance of the ectopic foci as presented in Fig. 10 [74].

5.2.2. Ventricular fibrillation without external stimulus

The route from normal functioning to ventricular fibrillation without external stimulus is now of concern. Table 1 shows that there are four different parameters comparing normal functioning and ventricular fibrillation without external stimulus: α_{HP}, $k^{\tau}{}_{SA-AV}$, k_{AV-HP}, $k^{\tau}{}_{AV-HP}$. The decrease of α_{HP} is presented in Fig. 25-a, showing two crucial changes along the variation: the first occurs close to $\alpha_{HP} = 3.5$ and the second close to $\alpha_{HP} = 3$. This diagram defines regions 1 to 3 with quasi-periodic responses. The decrease of parameter $k^{\tau}{}_{SA-AV}$ is presented in Fig. 25-b, and the region 3 remains up to $k^{\tau}{}_{SA-AV} = 2.25$. After this point, a cloud of points appears defining region 4, which presents some periodic windows. Fig. 25-c presents the decrease of parameter k_{AV-HP}, starting with region 5. The transition from region 6 to 7 is presented in Fig. 25-d, which is related to the decrease of $k^{\tau}{}_{AV-HP}$. Region 8 is related to the ventricular fibrillation.

Fig. 26 presents ECG time histories related to the regions discussed in Fig. 25. Responses related to regions 2 and 3 present an overlap of new waves after the P wave, showing disfunction of electrical activity of the heart. Time history associated with regions 4 and 5 present a higher frequency of beating when compared with the other responses presented in Fig. 26, both related to nonperiodic behaviors. Responses 7 and 8 are related to the decrease of $k^{\tau}{}_{AV-HP}$ and have no significant difference.

6. Conclusions

Cardiac rhythms are analyzed from a reduced-order mathematical model composed by three-coupled oscillators with time-delayed couplings. This model is capable to capture the main aspects of cardiac dynamical response, reproducing ECGs

for various situations of heart functioning, normal and pathological rhythms. Nonlinear dynamics perspective allows a proper investigation of the heart rhythm dynamics. Besides normal rhythms, the following pathologies are treated: atrial flutter, atrial fibrillation, ventricular flutter and two different kinds of ventricular fibrillation.

Lyapunov exponent estimation established the dynamical characteristics of each rhythm. Basically, normal rhythm, atrial and ventricular flutter are quasi-periodic responses while atrial and ventricular fibrillations are chaotic behaviors. Poincaré map construction is discussed pointing that it is an interesting tool to identify pathological rhythms. Two different approaches are proposed considering return map, based on a secant plane, and reference period, based on the frequency response. Both approaches providing similar conclusions showing that Poincaré maps allow one to identify different pathologies that are imperceptible from time series analysis. For example, the distinction between atrial flutter and atrial fibrillation or between ventricular flutter and ventricular fibrillation are more pronounced in state space plots. It should be pointed out that rhythm identification has ultimately a potential use for pathology diagnosis.

Bifurcation analysis is another nonlinear tool that can be useful to establish the route from normal functioning to pathological rhythms. Basically, bifurcations related of three different pathologies are investigated: atrial fibrillation; ventricular fibrillation with external stimulus; and ventricular fibrillation without external stimulus. The normal-pathological routes can also be employed for rhythm identification, being interesting to predict pathological behaviors before they are reached.

Acknowledgments

The authors would like to acknowledge the support of the Brazilian Research Agencies CNPq, CAPES and FAPERJ.

References

[1] M.A. Savi, Chaos and order in biomedical rhythms, J. Braz. Soc. Mech. Sci. Eng. 27 (2005) 157–169, doi:10.1590/S1678-58782005000200008.
[2] S.R.S.M. Gois, M.A. Savi, An analysis of heart rhythm dynamics using a three-coupled oscillator model, Chaos Solitons Fractals 41 (2009) 2553–2565, doi:10.1016/j.chaos.2008.09.040.
[3] L. Glass, Introduction to controversial topics in nonlinear science: is the normal heart rate chaotic? Chaos 19 (2009) 028501, doi:10.1063/1.3156832.
[4] D. Dubin, Interpretação Rápida Do ECG, EPUB, Rio de Janeiro, 1996.
[5] M. Malik, A.J. Camm, Heart Rate Variability, Futura, New York, 1995.
[6] G.K. Moe, W.C. Rheinboldt, J.A. Abildskov, A computer model of atrial fibrillation, Am. Heart J. 67 (1964) 200–220, doi:10.1016/0002-8703(64)90371-0.
[7] V.I. Krinsky, Mathematical models of cardiac arrhythmias (spiral waves), Pharmacol. Ther. Part B. 3 (1978) 539–555, doi:10.1016/S0306-039X(78)90020-X.
[8] F. Fenton, A. Karma, Vortex dynamics in three-dimensional continuous myocardium with fiber rotation: filament instability and fibrillation, Chaos 8 (1998) 20–47, doi:10.1063/1.166311.
[9] J. Jalife, O. Berenfeld, A. Skanes, R. Mandapati, Mechanisms of atrial fibrillation: mother rotors or multiple daughter wavelets, or both? J. Cardiovasc. Electrophysiol. 9 (1998) S2–S12 PMID: 9727669.
[10] F.H. Fenton, E.M. Cherry, H.M. Hastings, S.J. Evans, Multiple mechanisms of spiral wave breakup in a model of cardiac electrical activity, Chaos 12 (2002) 852–892, doi:10.1063/1.1504242.
[11] P.E. Mcsharry, G.D. Clifford, L. Tarassenko, L.A. Smith, A dynamical model for generating synthetic electrocardiogram signals, IEEE. Trans. Biomed. Eng. 50 (2003) 289–294, doi:10.1109/TBME.2003.808805.
[12] C.C. Mitchell, D.G. Schaeffer, A two-current model for the dynamics of cardiac membrane, Bull. Math. Biol. 65 (2003) 767–793, doi:10.1016/S0092-8240(03)00041-7.
[13] M.P. Nash, A.V. Panfilov, Electromechanical model of excitable tissue to study reentrant cardiac arrhythmias, Prog. Biophys. Mol. Biol. 85 (2004) 501–522, doi:10.1016/j.pbiomolbio.2004.01.016.
[14] B. van der Pol, J. van der Mark, The heartbeat considered as a relaxation oscillator and an electrical model of the heart, Philos. Mag. 6 (1928) 763–775, doi:10.1080/14786441108564652.
[15] K. Grudzinski, J.J. Zebrowski, Modeling cardiac pacemakers with relaxation oscillators, Physica A 336 (2004) 153–162, doi:10.1016/j.physa.2004.01.020.
[16] A.M. Dos Santos, S.R. Lopes, R.R.L. Viana, Rhythm synchronization and chaotic modulation of coupled Van der Pol oscillators in a model for the heartbeat, Physica A 338 (2004) 335–355, doi:10.1016/j.physa.2004.02.058.
[17] A. Cheffer, M.A. Savi, Random effects inducing heart pathological dynamics: an approach based on mathematical models, Biosystems 196 (2020) 104177, doi:10.1016/j.biosystems.2020.104177.
[18] E. Ryzhii, M. Ryzhii, Modeling of heartbeat dynamics with a system of coupled nonlinear oscillators, in: Proceedings of the International Conference on Biomedical Informatics and Technology, Berlin, Heidelberg, Springer, 2013, pp. 67–75, doi:10.1007/978-3-642-54121-6_6.
[19] E. Ryzhii, M. Ryzhii, A heterogeneous coupled oscillator model for simulation of ECG signals, Comput. Methods Programs Biomed. 117 (2014) 40–49, doi:10.1016/j.cmpb.2014.04.009.
[20] G.C. Cardarilli, L. Di Nunzio, R. Fazzolari, M. Re, F. Silvestri, Improvement of the cardiac oscillator based model for the simulation of bundle branch blocks, Appl. Sci. 9 (2019) 3653, doi:10.3390/app9183653.
[21] J. Son, D. Du, Y. Du, Stochastic modeling and dynamic analysis of the cardiovascular system with rotary left ventricular assist devices, Math. Probl. Eng. (2019), doi:10.1155/2019/7179317.
[22] D. Sato, R.E. Dixon, L.F. Santana, M.F. Navedo, A model for cooperative gating of L-type Ca_2+ channels and its effects on cardiac alternans dynamics, PLoS Comput. Biol. 14 (2018) e1005906, doi:10.1371/journal.pcbi.1005906.
[23] R.E. Dixon, C. Yuan, E.P. Cheng, M.F. Navedo, L.F. Santana, Ca2+ signaling amplification by oligomerization of L-type Cav1.2 channels, Proc. Natl. Acad. Sci. U.S.A. 109 (2012) 1749–1754, doi:10.1073/pnas.1116731109.
[24] M.A. Quiroz-Juárez, O. Jiménez-Ramírez, R. Vázquez-Medina, V. Breña-Medina, J.L. Aragón, R.A. Barrio, Generation of ECG signals from a reaction-diffusion model spatially discretized, Sci. Rep. 9 (2019) 1–10, doi:10.1038/s41598-019-55448-5.
[25] P. Pathmanathan, J.M. Cordeiro, R.A. Gray, Comprehensive uncertainty quantification and sensitivity analysis for cardiac action potential models, Front. Physiol. 10 (2019) 721, doi:10.3389/fphys.2019.00721.
[26] A.L. Goldberger, E. Goldberger, Clinical Electrocardiography, Mosby, St Louis, 1977.
[27] J. Pan, W.J. Tompkins, A real-time QRS detection algorithm, IEEE. Trans. Biomed. Eng. 3 (1985) 220–236, doi:10.1109/TBME.1985.325532.
[28] D.T. Kaplan, Simultaneous QRS detection and feature extraction using simple matched filter basis functions, In Proceedings Comp. Cardiol., IEEE. (1990) 503–506, doi:10.1109/CIC.1990.144266.
[29] G.B. Moody, R.G. Mark, A. Zoccola, S. Mantero, Derivation of respiratory signals from multi-lead ECGs, Comput. Cardiol. 12 (1985) 113–116.
[30] J.N. Herbschleb, R.M. Heethaar, I. Tweel, F.L. Meijler, Frequency analysis of the ECG before and during ventricular fibrillation, Comput. Cardiol. (1980) 365–368.

[31] P.S. Chen, A. Garfinkel, J.N. Weiss, H.S. Karagueuzian, Computerized mapping of fibrillation in normal ventricular myocardium, Chaos 8 (1998) 127–136, doi:10.1063/1.166293.
[32] P.V. Bayly, B.H. Kenknight, J.M. Rogers, E.E. Johnson, R.E. Ideker, W.M. Smith, Spatial organization, predictability, and determinism in ventricular fibrillation, Chaos 8 (1998) 103–115, doi:10.1063/1.166291.
[33] J. Jalife, Ventricular fibrillation: mechanisms of initiation and maintenance, Annu. Rev. Physiol. 62 (2000) 25–50, doi:10.1146/annurev.physiol.62.1.25.
[34] B. Nannes, R. Quax, H. Ashikaga, M. Hocini, R. Dubois, O. Bernus, M. Haïssaguerre, Early signs of critical slowing down in heart surface electrograms of ventricular fibrillation victims, in: Proceedings of the International Conference on Computational Science, Cham, Springer, 2020, pp. 334–347, doi:10.1007/978-3-030-50423-6_25.
[35] A.C. Skanes, R. Mandapati, O. Berenfeld, J.M. Davidenko, J. Jalife, Spatiotemporal periodicity during atrial fibrillation in the isolated sheep heart, Circulation 98 (1998) 1236–1248, doi:10.1161/01.CIR.98.12.1236.
[36] G. Krstacic, A. Krstacic, A. Smalcelj, D. Milicic, M. Jembrek-Gostovic, The chaos theory and nonlinear dynamics in heart rate variability analysis: does it work in short-time series in patients with coronary heart disease? Ann. Noninvas. Electro. 12 (2007) 130–136, doi:10.1111/j.1542-474X.2007.00151.x.
[37] J. Ernst, Z. Bar-Joseph, STEM: a tool for the analysis of short time series gene expression data, BMC Bioinform 7 (2006) 1–11, doi:10.1186/1471-2105-7-191.
[38] D.P. Tobón, S. Jayaraman, T.H. Falk, Spectro-temporal electrocardiogram analysis for noise-robust heart rate and heart rate variability measurement, IEEE J. Transl. Eng. Health Med. 5 (2017) 1–11, doi:10.1109/JTEHM.2017.2767603.
[39] Y. Shiraishi, Y. Katsumata, T. Sadahiro, K. Azuma, K. Akita, S. Isobe, F. Yashima, K. Miyamoto, T. Nishiyama, Y. Tamura, T. Kimura, N. Nishiyama, Y. Aizawa, K. Fukuda, S. Takatsuki, Real-time analysis of the heart rate variability during incremental exercise for the detection of the ventilatory threshold, J. Am. Heart Assoc. 7 (2018) e006612, doi:10.1161/JAHA.117.006612.
[40] Y. Wang, S. Wei, S. Zhang, Y. Zhang, L. Zhao, C. Liu, A. Murray, Comparison of time-domain, frequency-domain and non-linear analysis for distinguishing congestive heart failure patients from normal sinus rhythm subjects, Biomed. Signal Process. Control. 42 (2018) 30–36, doi:10.1016/j.bspc.2018.01.001.
[41] B. Hu, S. Wei, D. Wei, L. Zhao, G. Zhu, C. Liu, Multiple time scales analysis for identifying congestive heart failure based on heart rate variability, IEEE Access 7 (2019) 17862–17871, doi:10.1109/ACCESS.2019.2895998.
[42] H. Ueno, Y. Totoki, T. Matsuo. ECG characterization of sinus bradycardia and ventricular flutter using malthusian parameter and recurrence plot, ICIC-ELB. 9 (2018) 23–30. 10.24507/icicelb.09.01.23.
[43] M.D. Costa, A.L. Goldberger, Heart rate fragmentation: using cardiac pacemaker dynamics to probe the pace of biological aging, Am. J. Physiol. Heart Circ. Physiol. 316 (2019) H1341–H1344, doi:10.1152/ajpheart.00110.2019.
[44] M. Deng, C. Wang, M. Tang, T. Zheng, Extracting cardiac dynamics within ECG signal for human identification and cardiovascular diseases classification, Neural Netw 100 (2018) 70–83, doi:10.1016/j.neunet.2018.01.009.
[45] F. Silvestri, S. Acciarito, G.M. Khanal, Relationship between mathematical parameters of modified van der Pol oscillator model and ECG morphological features, Int. J. Adv. Sci. Eng. Inf. Technol. 9 (2019) 601–608, doi:10.18517/ijaseit.9.2.8296.
[46] A. Khan, M. Sulaiman, H. Alhakami, A. Alhindi, Analysis of oscillatory behavior of heart by using a novel neuroevolutionary approach, IEEE Access 8 (2020) 86674–86695, doi:10.1109/ACCESS.2020.2992281.
[47] D.T. Kaplan, R.J. Cohen, Is fibrillation chaos? Circ. Res. 67 (1990) 886–892, doi:10.1161/01.RES.67.4.886.
[48] F.E. Yates, L.A. Benton, Variance structure in the human cardiovascular system—Periodicity, chaos, or old-fashioned noise? Math. Comput. Model. 19 (1994) 161–170, doi:10.1016/0895-7177(94)90194-5.
[49] D.J. Christini, A. Kulkarni, S. Rao, E.R. Stutman, F.M. Bennett, J.M. Hausdorff, N. Oriol, K.R. Lutchen, Influence of autoregressive model parameter uncertainty on spectral estimates of heart rate dynamics, Ann. Biomed. Eng. 23 (1995) 127–134, doi:10.1007/bf02368320.
[50] Z. Bozóki, Chaos theory and power spectrum analysis in computerized cardiotocography, Eur. J. Obstet. Gynecol. Reprod. Biol. 71 (1997) 163–168, doi:10.1016/S0301-2115(96)02628-0.
[51] H. Kantz, T. Schreiber, Nonlinear Time Series analysis, vol. 7, Cambridge university press, 2004.
[52] R.M. Evaristo, A.M. Batista, L.R. Viana, K.C. Iarosz, J.D. Szezech Jr, M.F. Godoy, Mathematical model with autoregressive process for eletrocardiograma signals, Commun. Nonlinear Sci. Numer. Simul. 57 (2017) 415–421, doi:10.1016/j.cnsns.2017.10.018.
[53] J.Q. Zhang, A.V. Holden, O. Monfredi, M.R. Boyett, H. Zhang, Stochastic vagal modulation of cardiac pacemaking may lead to erroneous identification of cardiac chaos, Chaos 19 (2009) 028509, doi:10.1063/1.3141426.
[54] N. Wessel, M. Riedl, J. Kurths, Is the normal heart rate “chaotic” due to respiration? Chaos 19 (2009) 028508, doi:10.1063/1.3133128.
[55] T. Buchner, M. Petelczyc, J.J. Zebrowski, A. Prejbisz, M. Kabat, A. Januszewicz, W. Szelenberger, On the nature of heart rate variability in a breathing normal subject: a stochastic process analysis, Chaos 19 (2009) 028504, doi:10.1063/1.3152008.
[56] R.H. Johnstone, E.T. Chang, R. Bardenet, T.P. De Boer, D.J. Gavaghan, P. Pathmanathan, R.H. Clayton, G.R. Mirams, Uncertainty and variability in models of the cardiac action potential: can we build trustworthy models? J. Mol. Cell. Cardiol. 96 (2016) 49–62, doi:10.1016/j.yjmcc.2015.11.018.
[57] K.N. Aronis, R.D. Berger, H. Calkins, J. Chrispin, J.E. Marine, D.D. Spragg, S. Tao, H. Tandri, H. Ashikaga, Is human atrial fibrillation stochastic or deterministic? – Insights from missing ordinal patterns and causal entropy-complexity plane analysis, Chaos 28 (2018) 063130, doi:10.1063/1.5023588.
[58] J. Ibrahim, R. Staffeldt, Conley index methods detecting bifurcations in a modified van der Pol oscillator appearing in heart action models, arXiv 1901 (2019) 11180 https://arxiv.org/abs/1901.11180v1.
[59] A. Garfinkel, M.L. Spano, W.L. Ditto, J.N. Weiss, Controlling cardiac chaos, Science 257 (1992) 1230–1235, doi:10.1126/science.1519060.
[60] A. Garfinkel, J.N. Weiss, W.L. Ditto, M.L. Spano, Chaos control of cardiac arrhythmias Trends, Cardiovasc. Med. 5 (1995) 76–80, doi:10.1016/1050-1738(94)00083-2.
[61] E. Ott, C. Grebogi, J.A. Yorke, Controlling chaos, Phys. Rev. Lett. 64 (1990) 1196–1199, doi:10.1103/PhysRevLett.64.1196.
[62] B.B. Ferreira, A.S. De Paula, M.A. Savi, Chaos control applied to heart rhythm dynamics, Chaos Solitons Fractals 44 (2011) 587–599 2011, doi:10.1016/j.chaos.2011.05.009.
[63] B.B. Ferreira, M.A. Savi, A.S. De Paula, Chaos control applied to cardiac rhythms represented by ECG signals, Phys. Scr. 89 (2014) 105203, doi:10.1088/0031-8949/89/10/105203.
[64] F. Lounis, A. Boukabou, A. Soukkou, Implementing high-order chaos control scheme for cardiac conduction model with pathological rhythms, Chaos Solitons Fractals 132 (2020) 109581, doi:10.1016/j.chaos.2019.109581.
[65] M.A. Quiroz-Juarez, R. Vázquez-Medina, E. Ryzhii, M. Ryzhii, J.L. Aragón, Quasiperiodicity route to chaos in cardiac conduction model, Commun. Nonlinear Sci. Numer. Simul. 42 (2017) 370–378, doi:10.1016/j.cnsns.2016.06.007.
[66] A. Khan, U. Nigar, Combination projective synchronization in fractional-order chaotic system with disturbance and uncertainty, Int. J. Appl. Comput. Math. 6 (2020) 1–22, doi:10.1007/s40819-020-00852-z.
[67] B. Mensour, A. Longtin, Power spectra and dynamical invariants for delay-differential and difference equations, Physica D 113 (1998) 1–25, doi:10.1016/S0167-2789(97)00185-1.
[68] W.J. Cunningham, A nonlinear differential-difference equation of growth, Proc. Natl. Acad. Sci. U.S.A. 40 (1954) 708–713, doi:10.1073/pnas.40.8.708.
[69] PhysioNet Databases. https://physionet.org/about/database/, 2020. (acessed 10 December 2020).
[70] S. Canabrava, Eletrocardiografia, Med eLearning Cursos Interativos, Belo Horizonte, 2014.
[71] P. Brugada, J. Brugada, L. Mont, A new approach to the differential diagnosis of a regular tachycardia with a wide QRS complex, Circulation 83 (1991) 1649–1659, doi:10.1161/01.CIR.83.5.1649.
[72] O.A. Obel, A.J. Camm, Supraventricular tachycardia, Eur. Heart J. 18 (1997) 2–11, doi:10.1093/eurheartj/18.suppl_C.2.
[73] V. Fuster, L.E. Ryden, D.S. Cannom. H.J. Crijns, A.B. Curtis, K.A. Ellenbogen, J.L. Halperin, J.Y. Le Heuzey, G.N. Kay, J.E. Lowe, S.B. Olsson, E.N. Prystowsky, S.Wann J.L.Tamargo, S.C. Smith Jr, A.K. Jacobs, C.D. Adams, J.L. Anderson, E.M. Antman, J.L. Halperin, S.A. Hunt, R. Nishimura, J.P. Ornato, R.L. Page, B. Riegel, S.G. Priori, J.J. Blanc, A. Budaj, A.J. Camm, V. Dean, J.W. Deckers, C. Despres, K. Dickstein, John Lekakis, K. McGregor, M. Metra, J. Morais,

A. Osterspey, J.L. Zamorano, ACC/AHA/ESC 2006 guidelines for the management of patients with atrial fibrillation: a report of the American College of Cardiology/American Heart Association Task Force on practice guidelines and the European Society of Cardiology Committee for Practice Guidelines (Writing Committee to Revise the 2001 guidelines for the management of patients with atrial fibrillation) developed in collaboration with the European Heart Rhythm Association and the Heart Rhythm Society, Europace 8 (2006) 651–745, doi:10.1093/europace/eul097.

[74] G.J. Klein, T.M. Bashore, T.D. Sellers, E.L. Pritchett, W.M. Smith, J.J. Gallagher, Ventricular fibrillation in the Wolff-Parkinson-White syndrome, N. Engl. J. Med. 301 (1979) 1080–1085, doi:10.1056/NEJM197911153012003.